Sedimentary Geology 435 (2022) 106155

Contents lists available at ScienceDirect

Sedimentary Geology

journal homepage: www.elsevier.com/locate/sedgeo

Mid-latitude alluvial and hydroclimatic changes during the Paleocene–Eocene Thermal Maximum as recorded in the Tremp-Graus Basin, Spain

Aitor Payros [a,*], Victoriano Pujalte [a], Birger Schmitz [b]

[a] Department of Geology, Faculty of Science and Technology, University of the Basque Country UPV/EHU, Ap. 644, E-48080 Bilbao, Spain
[b] Department of Physics, University of Lund, P.O. Box 118, SE-221 00 Lund, Sweden

ARTICLE INFO

Article history:
Received 4 February 2022
Received in revised form 11 April 2022
Accepted 16 April 2022
Available online 21 April 2022

Editor: Dr. Catherine Chagué

Keywords:
PETM
Palaeoclimate
Alluvial architecture
Claret Conglomerate
Yellowish Soils
Palaeosols

ABSTRACT

A short episode (~170 kyr) of extremely high global temperatures that occurred ~56 Ma, known as the Paleocene–Eocene Thermal Maximum, is widely considered an ancient analogue of the ongoing anthropogenic warming. This ancient hyperthermal event consisted of three phases, onset, core and recovery, which are respectively represented in the mid-latitude south Pyrenean Tremp-Graus Basin by three successive terrestrial units, the Claret Conglomerate, the Yellowish Soils and the Gypsum-rich Unit, each of them recording a different sedimentary response to evolving climatic and hydrological regimes. The Claret Conglomerate is mainly made up of calcareous conglomerates and is acknowledged to record an abrupt hydrological change during the onset phase. This unit most likely formed in an alluvial megafan, an interpretation here reinforced with new architectural information and by comparison with naturally occurring small-scale fan-like accumulations. Assuming the similarity between the onset of the Paleocene–Eocene Thermal Maximum and the anthropogenic warming, recent hydrological and meteorological data from mid-latitude Spain were compiled for comparison purposes. This comparison concurs with published modelling results about hydroclimate changes in the Pyrenees during the hyperthermal event, postulating an enhancement of seasonal contrast with augmented frequency and intensity of floods but no significant change in total rain. Furthermore, the comparison suggests that the Claret Conglomerate accumulated during extreme rainfall episodes that mainly occurred in autumn. The Yellowish Soils are mostly composed of silty marls with ubiquitous small-sized carbonate nodules and intercalated calcarenites. The marls were deposited in floodplains and the calcarenites in point bars and crevasse splays of meandering rivers. The scarcity of conglomerates entails a near absence of strong currents, and the carbonate nodules perennial or seasonal arid conditions. These nodules occur within cumulate palaeosols, the development of which required regular sedimentary increments during inundations on the floodplains. Sedimentation rates of siliciclastic material on the floodplains increased significantly during the core of the hyperthermal event, as well as at river outlets in coastal settings, which shows that erosion was accelerated and rules out the occurrence of protective, dense vegetation. Combined, these characteristics suggest persistent very dry summers, but a smooth wet season without intense precipitation events. Lastly, the profusion of gypsum in the youngest unit is clear proof of an arid climate during the recovery of the hyperthermal event. In essence, the studied deposits provide a unique window into the sequence of hydroclimatic change during the rise, peak and decline of an ancient global warming event in a mid-latitude terrestrial setting, against which ongoing climate-change data and future projections can be compared.

1. Introduction

A massive emission of light carbon into the atmosphere and oceans about 56 Ma caused a ~170 kyr long episode of intense global warming known as the Paleocene–Eocene Thermal Maximum (PETM). The hyperthermal event, recorded in marine and terrestrial sedimentary archives by a negative carbon isotope excursion, is widely considered an ancient analogue of the ongoing anthropogenic warming of the Earth (Thomas and Zachos, 2000; Sluijs et al., 2007; Zachos et al., 2008; McInerney and Wing, 2011; Alley, 2016; Tierney et al., 2020).

One of the effects of the PETM was an alteration of the global hydrological cycle. Both geological proxy data and model simulations have shown that the hydrological changes varied geographically, producing aridification in some areas but greater precipitation in others (e.g., Carmichael et al., 2017; Lunt et al., 2017). The latter resulted in increased influx of terrestrial clastics into widely separated shallow

* Corresponding author.
E-mail address: a.payros@ehu.eus (A. Payros).

https://doi.org/10.1016/j.sedgeo.2022.106155

marine shelves and continental margins (e.g., Gibson et al., 2000; Schmitz et al., 2001; John et al., 2008; Slotnick et al., 2012; Pujalte et al., 2015, 2016, 2019; Pujalte and Schmitz, 2019; Jiang et al., 2021). Terrestrial sedimentary archives, despite being less extensive than marine records, have a higher sensitivity to hydrological changes, as variations in rainfall in catchment areas rapidly modify the pattern of river flows and the features of their deposits (Cecil and Dulong, 2003). For instance, in the Piceance Creek Basin of Colorado, in the Uinta Basin of Utah and in the San Juan Basin of New Mexico (USA), abrupt alterations in the architecture of fluvial deposits during the PETM are attributed to a coeval hydroclimate change (Foreman et al., 2012; Foreman, 2014; Plink-Björklund et al., 2014; Zellman et al., 2020).

The PETM is represented in the Tremp-Graus Basin (southern Pyrenees, Spain) by three terrestrial units, the Claret Conglomerate, the Yellowish Soils, and the Gypsum-rich Unit. The Claret Conglomerate is a sheet-like extensive unit 0.5–7 m thick, first described by Schmitz and Pujalte (2007), that has been used by several authors to infer the effects of the PETM hydrological change (e.g., Schmitz and Pujalte, 2007; Pancost, 2017; Armitage et al., 2011, 2013; Carmichael et al., 2017, 2018; Colombera et al., 2017; Chen et al., 2018). However, the precise depositional setting of the Claret Conglomerate is still somewhat controversial, as both megafan and braided fluvial models have been considered (Schmitz and Pujalte, 2007; Colombera et al., 2017). The Yellowish Soils are up to 20 m thick and mostly made up of silty calcareous clays with intercalated calcarenites. The Gypsum-rich Unit is up to 10 m thick and, as implied by its name, contains abundant gypsum deposits. Although the contrasting lithological character of these three units intuitively suggests a sequence of hydroclimatic changes during the PETM, this possibility has received little attention to date.

The purpose of this paper is to establish the depositional conditions of the three constituent units of the PETM in the Tremp-Graus Basin, a crucial information to assess properly the impact of hydrological changes associated to the hyperthermal event. New field studies were conducted in two sectors of the Tremp-Graus Basin, Esplugafreda and Claret, which respectively correspond to the most proximal and distal outcrops available for the target units. The former sector is located on the southern margin of the Esplugafreda ravine and provides a ~3 km long near-continuous exposure of the entire Tremp Group. The latter sector is situated around the Claret hamlet, about 2.5 km to the southwest of the city of Tremp (Fig. 1). Prior data of Schmitz and Pujalte (2007) and Pujalte et al. (2014) from other nearby sections (e.g., Berganuy, Iscles, Serraduy) have also been taken into account.

Model predictions of the response of Earth's climate to anthropogenic carbon emissions suggest an intensified hydrological cycle in arid to semiarid mid-latitude regions. Assuming the similarity between the PETM and the anthropogenic warming, our empirical observations can be crucial in calibrating model simulations of precipitation patterns and the sedimentary response in Earth's future greenhouse world.

2. Setting and previous information

2.1. Palaeogeography

During the Paleocene–Eocene boundary interval the Tremp-Graus Basin was located at ~35°N palaeolatitude, on the southeastern margin of an E–W elongated marine embayment surrounded by coastal alluvial plains (Fig. 1A) (Plaziat, 1981; Baceta et al., 2011). The basin was created and transported piggy-back on top of a thrust sheet during a Santonian—Maastrichtian interval of compressional tectonism (Burbank et al., 1992; Ardèvol et al., 2000; Fernández et al., 2012; Chanvry et al., 2018). During the tectonically quiescent late Maastrichtian—earliest Ypresian interval the basin had a steep northern margin on the forelimb of the Nogueres thrust and a gentle southern margin on the backlimb of the Montsec thrust (Fig. 1B). During the main compressional Ypresian—Oligocene interval, the basin was deformed, uplifted, and most of its northern part eroded away (Teixell and Muñoz, 2000).

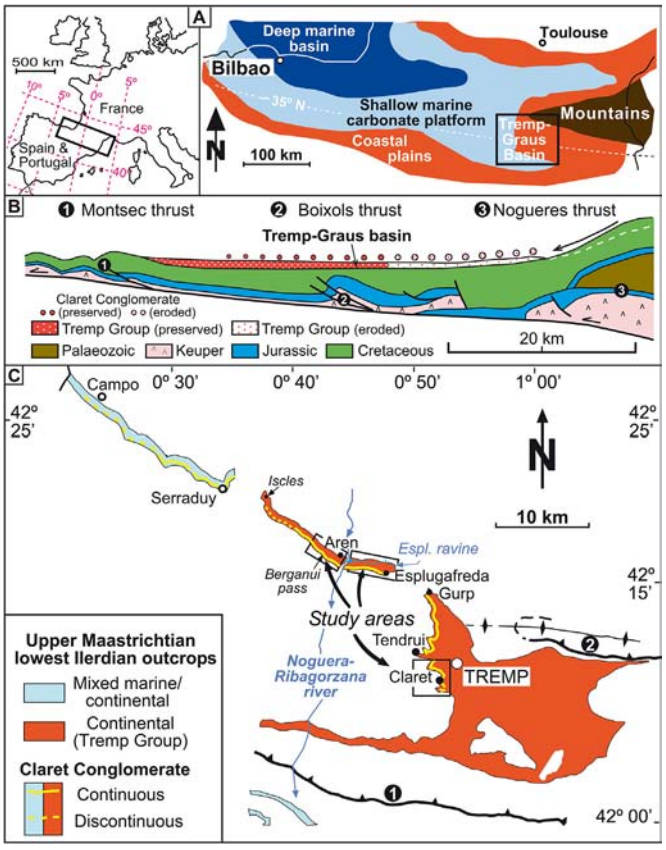

Fig. 1. (A) Location and simplified early Paleogene palaeogeography of the Pyrenean domain. (B) Reconstructed early Eocene cross-section along the Noguera Ribagorzana river valley (modified after Teixell and Muñoz, 2000). (C) Outcrop map of the Tremp-Graus Basin, with location of the Esplugafreda and Claret sectors and reference sections mentioned in the text.

2.2. Stratigraphy

The eastern part of the Tremp-Graus Basin was mostly infilled with terrestrial clastic deposits, informally named "Garumnian" (Rosell et al., 2001) and formally Tremp Group (Puigdefabregas et al., 1989; Cuevas, 1992; Dreyer, 1993; Pujalte and Schmitz, 2005; Pujalte et al., 2014). These terrestrial deposits overlie the transitional Aren Sandstone Formation (Maastrichtian), are overlain by the shallow marine "Alveolina limestone" (lower Ypresian), and interfinger to the west with lacustrine and shallow marine carbonates (Fig. 1C) (Serra-Kiel et al., 1994; Pujalte et al., 2014). In the two studied sectors the Thanetian to lowermost Ypresian interval comprises two lithostratigraphic units, the Esplugafreda and Claret formations (Figs. 2, 3A, B) (Cuevas, 1992; Dreyer, 1993; Pujalte and Schmitz, 2005; Pujalte et al., 2014).

The Esplugafreda Formation (Thanetian) is ~165 m thick at Esplugafreda and ~350 m thick at Claret. In both sectors the unit is mostly made up of overbank red silty marls with intercalated channels infilled with calcareous conglomerates and calcarenites (Fig. 2A, D). The channels occur either isolated or in laterally connected strings, in both cases successive channels occupying slightly higher stratigraphic positions (Fig. 3B). At Esplugafreda the red marls contain *Microcodium* (submillimetre-sized monocrystalline prisms of calcite originated on roots of terrestrial plants; Klappa, 1978, 1980; Košir, 2004; Kabanov et al., 2008), gypsum horizons and abundant palaeosol carbonate nodules, 1.5–3 cm in diameter, usually concentrated in discrete palaeosol horizons. (Fig. 2A, C). Carbonate nodules are less abundant at Claret but gypsum is widespread, including accumulations up to 10 m thick, deposited in saline lakes or continental sabkhas (García Veigas, 1997).

The Claret Formation contains five successive members (Fig. 2A, B), briefly described below from older to younger. Member 1 comprises

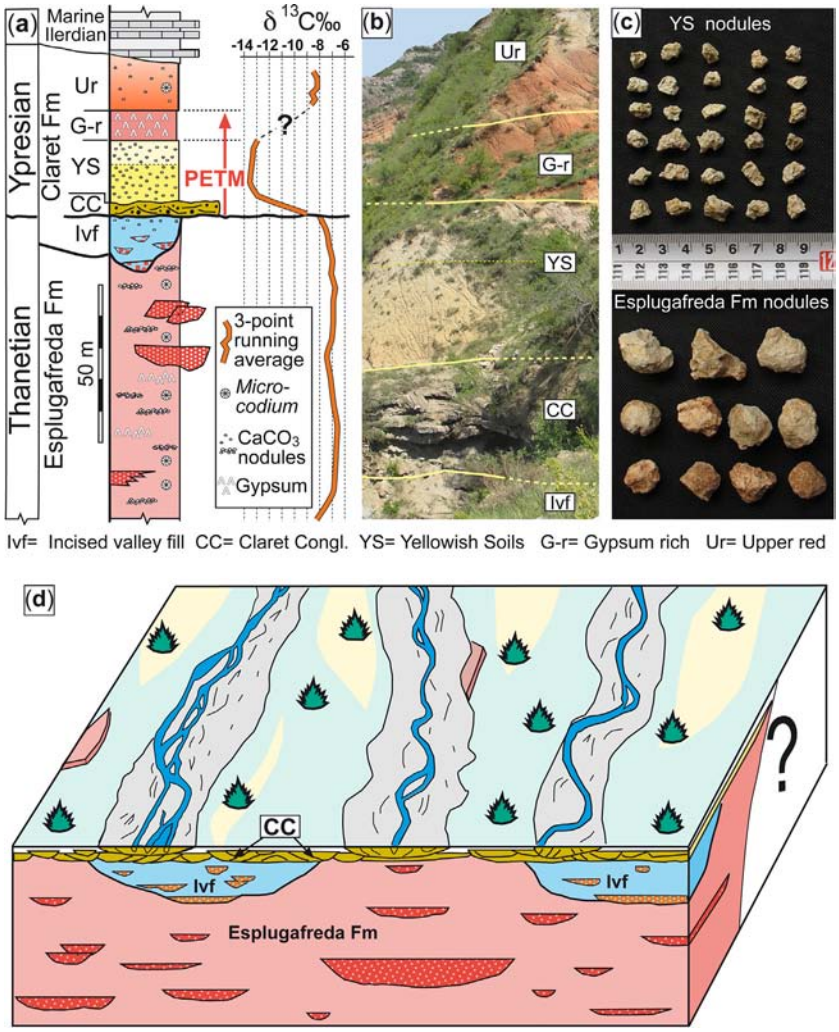

Fig. 2. (A) Synthetic lithostratigraphy and $\delta^{13}C$ isotopic profile of the Paleocene–Eocene interval in the Esplugafreda sector (modified from Pujalte et al., 2014). (B) Field view of the Claret Formation lithological units. (C) Representative carbonate nodules of the Esplugafreda Formation and the Yellowish Soils. (D) Simplified block diagram by Colombera et al. (2017; redrawn from part of their Fig. 13) showing the palaeogeographic reconstruction of the Esplugafreda sector during the deposition of the Claret Conglomerate.

the deposits infilling several incised valleys, 1–1.5 km wide and 20–30 m deep, excavated during a lowstand period predating the PETM. These valleys, which are floored by calcareous conglomerates and coarse-grained pebbly calcarenites, were mostly filled-up by pale red marls with sparse carbonate nodules at Esplugafreda and by light grey calcarenites and marlstones rich in coal remains at Claret (Pujalte et al., 2014, 2022).

Member 2, the Claret Conglomerate, is an extensive sheet-like unit, 0.5–7 m thick, of clast-supported calcareous conglomerates, pebbly calcarenites and minor marls (Figs. 2D, 3A, B; Supplementary Fig. 1). The genesis of sheet-like clastic accumulations is commonly attributed to a reduction in accommodation space during tectonically quiescent intervals (e.g., Heller and Paola, 1989). Although tectonic conditions in the Tremp-Graus Basin were quiescent during the entire late Maastrichtian—early Ypresian interval (Fernández et al., 2012), only the Claret Conglomerate shows sheet-like geometry. Hence, Schmitz and Pujalte (2007) attributed the development of the Claret Conglomerate to an abrupt increase of clastic supply caused by the PETM hydrologic change.

Member 3, the Yellowish Soil unit, is up to 20 m thick and mainly consists of silty marls with occasional intercalations of calcarenites. In weathered outcrops, the lower part of the silty marls has a yellow-orange colour, which up section becomes increasingly lighter (Fig. 2A, B). Neither *Microcodium* nor gypsum have been observed, but the marls contain abundant small-sized (0.5–1 cm) palaeosol carbonate nodules dispersed throughout the unit (Fig. 2A, C).

Member 4, the Gypsum-rich Unit, is represented at Esplugafreda by deep-red marls that include numerous gypsum crystals and veins (Fig. 3C), and at Claret by a massive package of alabastrine gypsum up to 4 m thick (Fig. 3D). Neither conglomerates nor calcarenites have been observed in any outcrop of the unit.

Member 5, the upper red unit, only exists at Esplugafreda, where it is up to 17 m thick and comprises light red marls with dispersed carbonate nodules and occasional *Microcodium*. The overlying "Alveolina limestone" is a time-transgressive marine unit, which onlaps member 4 at Claret and member 5 at Esplugafreda (Fig. 2A).

2.3. The PETM in the Tremp-Graus Basin

The PETM was first constrained in the Tremp-Graus Basin with $\delta^{13}C$ isotopes from palaeosol carbonate nodules of the Esplugafreda Formation, the incised valley fill, the Yellowish Soils and the upper red unit (Schmitz and Pujalte, 2003). Later, carbonate nodules were also found in red marls intercalated within the Claret Conglomerate, which produced $\delta^{13}C$ values intermediate between those of the Esplugafreda Formation/incised valley fill and the Yellowish Soils (Schmitz and Pujalte, 2007). These data showed that the bulk of the Esplugafreda Formation

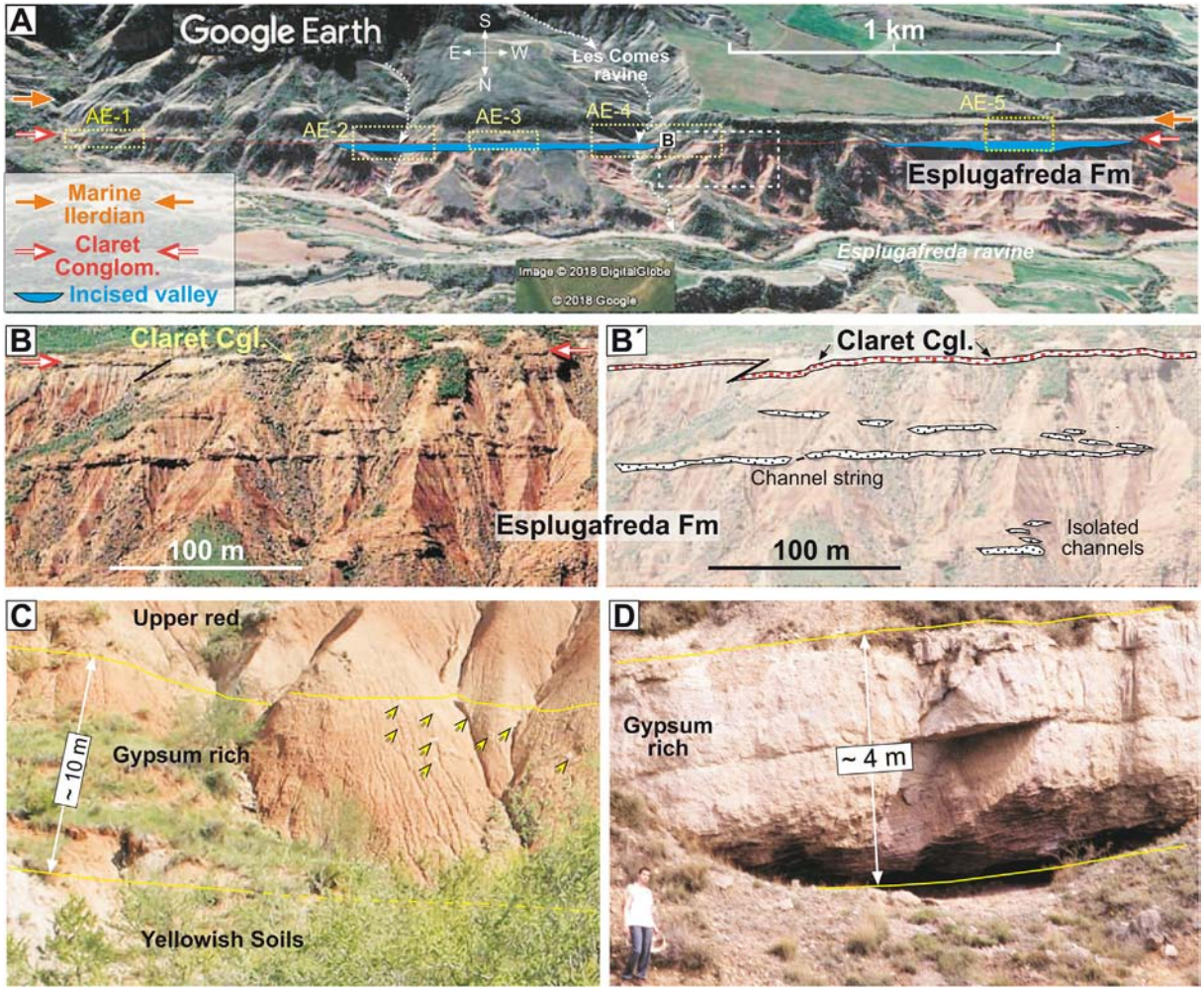

Fig. 3. (A) Panoramic Google Earth/Digital Globe image of the Paleocene–lower Eocene outcrop in the Esplugafreda sector, with indication of the lithostratigraphic units differentiated by Pujalte et al. (2014) and the location of the Architectural Ensembles (AE) recognized in this study. (B, B') Enlarged view of part of the outcrop (location in (A)) illustrating the contrasting large-scale architecture of coarse clastic channels intercalated in the Esplugafreda Formation and the Claret Conglomerate. (C, D) Field views of the Gypsum-rich Unit at the Esplugafreda sector (some gypsum crystals indicated by arrows) and at the Claret sector.

and the incised valley fill deposits predate the PETM, the Claret Conglomerate and the Yellowish Soils encompass the onset and core of the hyperthermal event, respectively, and the Gypsum-rich Unit records the recovery to background conditions (Fig. 2A). Subsequent $\delta^{13}C$ isotope studies of bulk dispersed organic carbon essentially agree with that conclusion (Domingo et al., 2009; Manners et al., 2013; Pujalte et al., 2022).

Measurements of cross stratifications, clast imbrication, and sole marks by Dreyer (1993) and Colombera et al. (2017) at the Esplugafreda sector indicate southward and southwestward palaeocurrents, an evidence that the E-W Esplugafreda outcrop provides a near strike view of the Thanetian—lower Ypresian terrestrial succession. Puigdefabregas et al. (1989) and Dreyer (1993) interpreted this entire succession as fluviatile, ascribing the vertical variations in the proportion of conglomerates to changing tectonic conditions. Schmitz and Pujalte (2007) considered that the Claret Conglomerate represents the extensive braidplain of a megafan caused by an abrupt increase in clastic supply during episodic high-energy rainstorms, severe floods and greater avulsion frequency related to enhanced seasonality during the PETM onset. Instead, Colombera et al. (2017) attributed the differences between the Claret Conglomerate and the underlying deposits to the development of a braided fluvial network (Fig. 2D), an interpretation that will be discussed below.

Kiehl et al. (2018) modelled the climatic conditions of the Pyrenees in pre-PETM and PETM times using the Community Climate System Model framework, and compared their results with published proxy data from the area. They concluded that the Pyrenees experienced enhanced seasonal amplitude in surface air temperature during the PETM, which produced increased summer warming by 8 °C. As a consequence, summer evaporation also increased, causing excessive drying from June to August. Seasonal precipitation increased by 50–200%, maximum increase in rainfall occurring from October to January. However, if maximum orbital forcing was also considered, the largest increase in run-off was modelled in August, September and October.

Chen et al. (2018), also based on data from the Esplugafreda sector, calculated that water discharge increased between 1.35 and 14 times during the formation of the Claret Conglomerate. For their calculation, they measured the b-axes of more than 5000 clasts, the depth and width of 48 channels from the Esplugafreda Formation, the incised valley deposits and the Claret Conglomerate, and took into account data of channel dimensions from Dreyer (1993) and Colombera et al. (2017). They found that the 50th percentile (D_{50}) of clast size distributions in pre-PETM deposits was 21.2 ± 5 mm, slightly diminishing to 19.5 ± 4 mm in the Claret Conglomerate. As per channel dimensions, it should be noted that the only "Claret Conglomerate channels" illustrated by these authors, in their supplementary Fig. 2, are from line drawings reproduced from Dreyer (1993). These channels, however, do not belong to the Claret Conglomerate, but to the basal conglomeratic deposits of one of the incised valleys (Supplementary Fig. 2), an error that casts doubt on the accuracy of their calculations.

3. Material and methods

This study is chiefly based on fieldwork focused on the Claret Conglomerate, the Yellowish Soils and the Gypsum-rich Unit. For the study of the Claret Conglomerate our emphasis was placed on the large-scale geometries of coarse-grained deposits, instead of focusing only on clast sizes, sedimentary structures, barforms or dimensions of individual channels. Thus, the entire ~3 km long outcrop of the Claret Conglomerate in the Esplugafreda sector was walked along and its best-exposed segments mapped and measured in detail. As a result, laterally continuous tracks of the unit, up to 350 m wide and plausibly having palaeogeomorphic significance, were differentiated. These tracts are here named "Architectural Ensembles" (AE), because their main distinctive features are thickness and internal sedimentary geometries (Fig. 4). The size of the largest clasts was routinely measured in most outcrops. Photomosaics and Google Earth images were used to map large-scale differences between the Claret Conglomerate and the coarse-grained clastic units of the underlying deposits (Fig. 3A, B; Supplementary Fig. 2).

The same approach could not be applied in the Claret sector, as several segments of the Claret Conglomerate are inaccessible or poorly exposed. However, field mapping of selected outcrops in strike and dip sections permitted a reasonably accurate reconstruction of the architecture of the unit in this sector. Palaeocurrents at Claret were determined from clast imbrications and cross-stratifications.

The Yellowish Soils and the Gypsum-rich units are not as well exposed as the Claret Conglomerate, often being overgrown with vegetation due to their predominantly fine-grained lithology. For this study, their best outcrops were carefully mapped in both studied sectors. Special attention was paid to the character of the calcarenites intercalated in the silty marls of the Yellowish Soils and to the stratigraphic relationships between the Yellowish Soils and the Claret Conglomerate. In addition, given that palaeosol colour can have compositional significance (Eppes and Johnson, 2022), four samples were collected from the silty marls of the Yellowish Soils, homogeneously distributed in ascending stratigraphic order. The samples were ground to powder using an agate mortar and stored in transparent, antiglare prismatic vials. The colour of the powder samples was visually determined following the Munsell system of hue, value and chroma, using a standard rock-colour chart (Munsell Color, 2009). These determinations were further verified using colour analysis software. To this end, the powder vials were scanned at high resolution (600 dpi) using a desktop office scanner in a dark room. Eight RGB measurements were made on each sample and mean RGB values were converted into the corresponding Munsell colour keys using available calibration tables (Centore, 2013).

4. Results

4.1. Esplugafreda sector

4.1.1. Claret Conglomerate

The features of the Claret Conglomerate at Esplugafreda and neighbouring outcrops change laterally. Its thickness, for instance, decreases from about 7 m near the Gurp and Esplugafreda hamlets to about 2 m just to the east of the Noguera-Ribagorzana River (Fig. 1C; Supplementary Fig. 1A, B). To the west of this river, the thickness of the unit increases to about 8 m at the Berganuy pass and then diminishes again, eventually pinching-out near the abandoned Iscles hamlet (Supplementary Fig. 1B, D). The Claret Conglomerate reappears near the Serraduy village, further west decreasing in thickness and becoming discontinuous (Fig. 1C; Supplementary Fig. 1E). Both in the Serraduy and Berganuy pass areas, the base of the Claret Conglomerate is essentially flat and its top slightly convex-up, an observation extrapolated to the entire unit to explain its lateral thickness variations (Supplementary Fig. 1B, C).

The deposits of the Claret Conglomerate are generally clast-supported, ungraded or with poorly defined inverse grading (Supplementary Fig. 3A, B). However, stacked, decimetre-scale cycles of conglomerates grading up into calcarenites also occur (Supplementary Fig. 3C). The nature and size of the clasts also vary laterally. Thus, along the Esplugafreda outcrop grey clasts are predominant, probably derived from upper Cretaceous carbonates, and clast diameters larger than 20 cm are rare. Conversely, in the Berganuy pass section clasts with 30–60 cm long axes are common, some of them reaching ca. 80 cm (Supplementary Figs. 3, 4B). Their lithologies are also more varied as, in addition to upper Cretaceous grey carbonates, lower Cretaceous orbitolinid-rich clasts and reddened Maastrichtian clasts are also common. These changes indicate that the Claret Conglomerate was fed through several source points, as implied in Fig. 1D of Schmitz and Pujalte (2007) and explicitly stated by Colombera et al. (2017). The detailed analysis of the Esplugafreda outcrop carried out in this study has revealed other lateral variations in the Claret Conglomerate, based on which five different architectural ensembles (AE) have been differentiated (Figs. 3A, 4), their main features being described below from east to west.

AE-1 comprises several exposures along a ~300 m wide tract in the easternmost part of the Esplugafreda valley (Fig. 3A). The Claret Conglomerate is 6–7 m thick in this ensemble (Figs. 4, 5) and mostly composed of stacked packages, a few meters wide and about 1 m thick, of conglomerates bounded by concave-up, cross-cutting erosional surfaces (Fig. 5B, C). The conglomerates lack grading, segregation or other

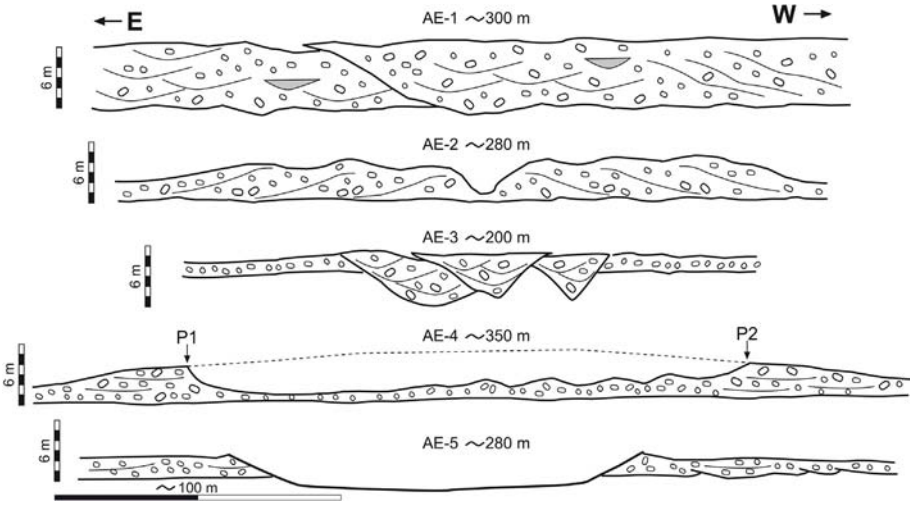

Fig. 4. Simplified sketches of the five Architectural Ensembles recognized in this study (explanation in the text).

internal organization, the long axes of their clasts being up to 20 cm, but generally smaller. Some shallow scours are infilled with calcarenites and dark-grey marls rich in plant remains (Fig. 4). Large-scale cross-strata inclined nearly perpendicular to the south-directed palaeocurrents are visible in one of the outcrops (Fig. 5D).

AE-2 is continuously exposed for about 280 m to the east and west of an unnamed ravine (Figs. 3A, 6A). The ensemble is up to 4.6 m thick and consists of conglomerates and calcarenites arranged in laterally accreted, low angle inclined strata separated by thin mudstone partings (Fig. 4). Notably, lateral accretion is oriented in opposite directions on each side of the ensemble, to the east on the eastern flank (Fig. 6B) and to the west on the western side (Fig. 6C). The thickness of individual strata varies laterally, some of them ending in gross bulges of cross-bedded conglomerates and pebbly sandstones, their palaeocurrents being concurrent with the direction of accretion (Fig. 6D, E). A channel-like depression about 10 m wide and 3 m deep separates both flanks (Fig. 4).

AE-3 is the only ensemble in which individual channels can be clearly delineated, as they are partly encased in marls (Figs. 4, 7). It contains three channels infilled with conglomerates, calcarenites and minor

Fig. 5. (A) Map of the Claret Conglomerate Architectural Ensemble-1 on a Google Earth/Digital Globe image (location in Fig. 3A). (B–D) Field photos of selected outcrops of the Ensemble (location in (A)). Thickness of the Claret Conglomerate is ~6 m in (B), and ~7 m in (C) and (D). Explanation within the text.

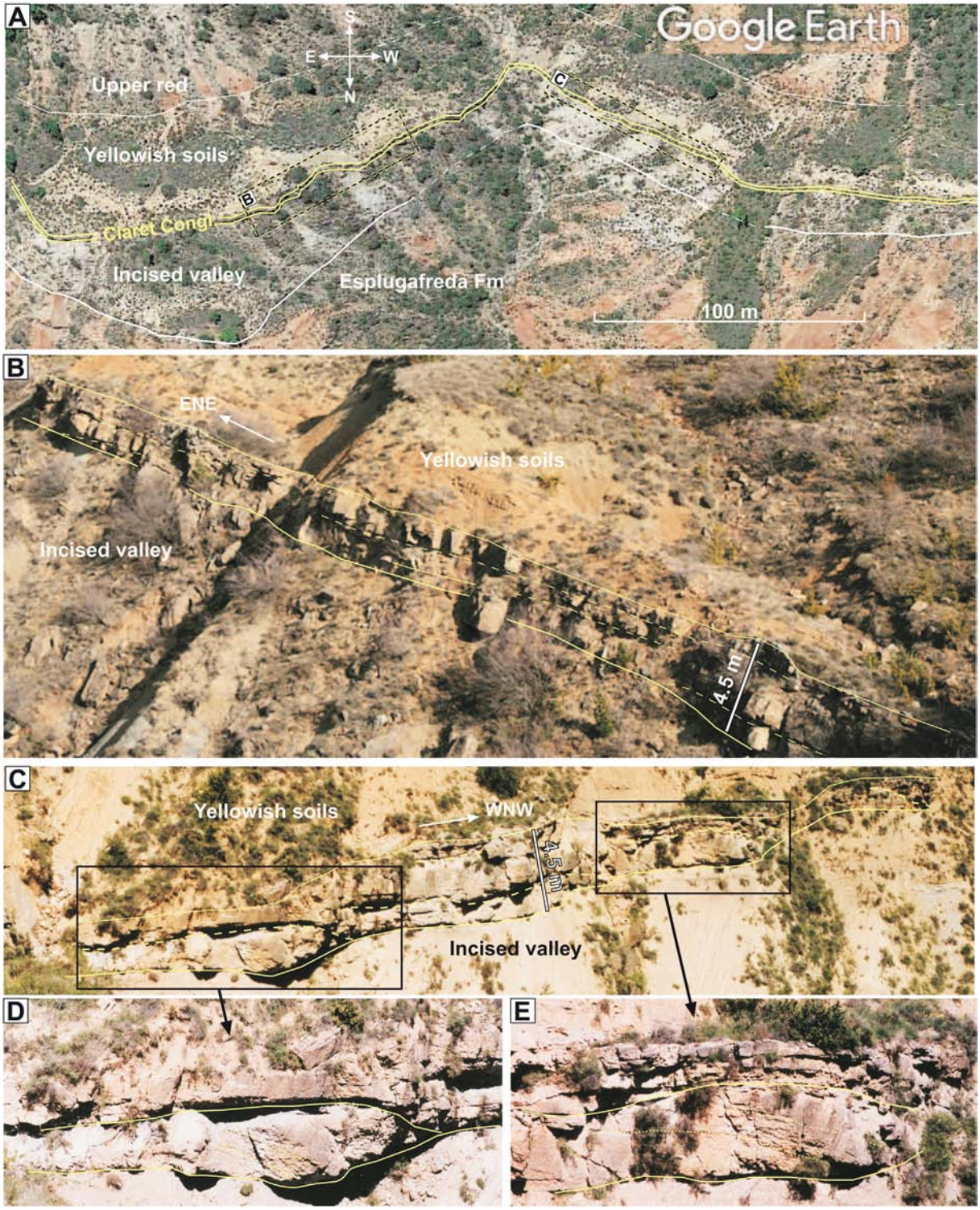

Fig. 6. (A) Map of the Claret Conglomerate Architectural Ensemble-2, and of its underlying and overlying units, on a Google Earth/Digital Globe image (location in Fig. 3A). (B, C) Field photos of the Ensemble's eastern and western branches. (D, E) Close-ups of selected parts of the western branch. Explanation within the text.

marls. Width/depth dimensions are 23/4.5 m in channel 1 and about 50/3 m in channels 2 and 3. Channel 3 is located between the other two, partly overlapping them (Fig. 7A). To the east and west of the channels, the ensemble is ≤2 m thick and has a tabular shape (Figs. 4, 7A).

AE-4, which is more than 350 m wide, is exposed across the Les Comes creek, a side-valley of the Esplugafreda ravine (Fig. 3A). The thickness, lithology and morphology of the ensemble change laterally (Figs. 4, 8). Thus, at reference points P1 and P2 in Fig. 8A the Claret Conglomerate is about 3 m thick and mostly made up of conglomerates, its thickness slightly declining to the east and west of both points (Fig. 4). However, between these two points the Claret Conglomerate has a smaller thickness, so that a sort of topographic depression about 200 m wide is recognized (Fig. 8A). On the western side of the depression the decrease in thickness is gradual, and different zones are

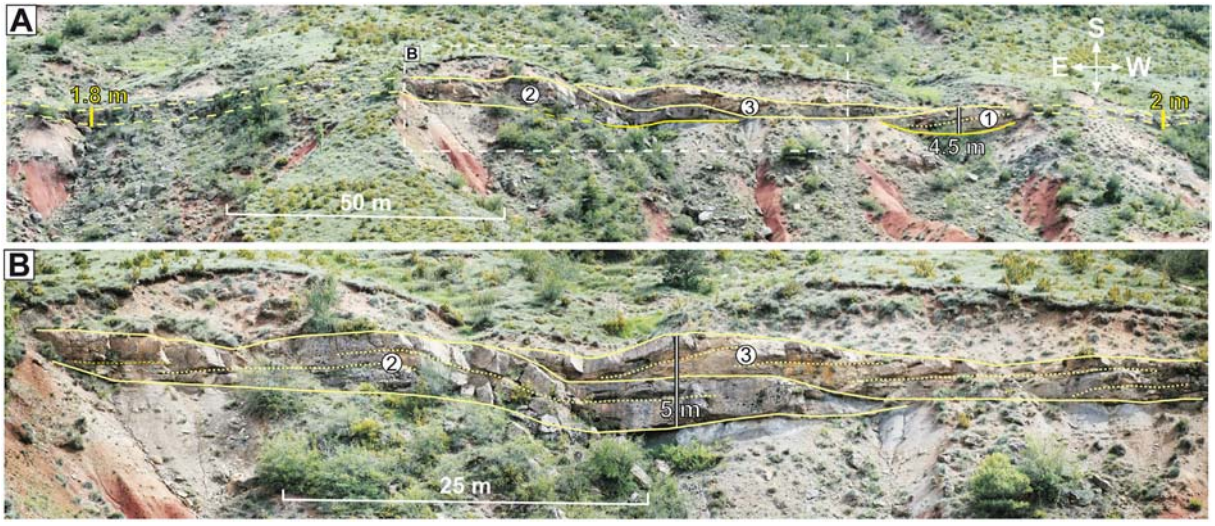

Fig. 7. General view (A) and close-up (B) of the channelized central part of the Claret Conglomerate Architectural Ensemble-3 (location in Fig. 3A). Explanation within the text.

recognizable. In effect, between points P2 and P3 the Claret Conglomerate is still mostly composed of conglomerates that have a flat base and an undulating top, its thickness varying from up to 2 m in the crests to less than 0.6 m in the inter-crest lows (Fig. 8B). The thickness of the Claret Conglomerate further decreases to about 1 m between points P3 and P4, where the unit is made up of conglomerates and pebbly calcarenites arranged in laterally accreted, low-angle inclined strata, and diminishes to a minimum of ~0.5 m between points P4 and P5 (Fig. 8C). In contrast, just west of reference point P1, on the eastern side of the depression, the thickness of the Claret Conglomerate rapidly diminishes from 3 to 1.5 m along a near straight line striking NNE–SSW, creating a smooth cliff (Fig. 8D, E, Supplementary Fig. 4A).

AE-5, which is situated in the western part of the Esplugafreda outcrop, is about 280 m wide and mostly overlies incised valley deposits (Figs. 3A, 9A). It is mainly composed of near tabular conglomerates 2–2.5 m thick (Fig. 4) that, in parts of the ensemble, exhibit a sort of lateral accretion arrangement in which successive strata terminate abruptly against the underlying incised valley deposits (Fig. 9B). The most distinctive feature of the ensemble, however, is an erosional depression about 150 m wide situated in its central part, within which the Claret Conglomerate has been completely removed, so that Yellowish Soil calcarenites rest directly on the incised valley deposits (Fig. 9A, C).

4.1.2. Yellowish Soils

In most of the Esplugafreda and Berganuy pass sectors the Claret Conglomerate is directly overlain by friable silty marls (i.e., the Yellowish Soils), which have been partly removed by recent erosion. As a result, the top of the Claret Conglomerate is widely exposed at several places as a sharp surface with a gentle convex-up geometry (Supplementary Fig. 4A, B).

Despite the distinctive colour of the Yellowish Soils, the silty marls show different shades of yellow at different stratigraphic levels, as they progressively become lighter coloured upsection (Figs. 2B, 6B). Using the Munsell colour key, the lower half of the Yellowish Soils shows yellowish grey (5Y 7/2) and moderate yellowish brown (10YR 5/4) colours, whereas the upper part shows greyish orange (10YR 7/4) to pale yellowish orange (10YR 8/6) colours (Supplementary Fig. 5). These determinations show that the Yellowish Soils are characterized by progressively higher chroma upsection.

Locally, the Yellowish Soils also contain calcarenite beds, which rest directly either on the Claret Conglomerate or, exceptionally, on incised valley deposits. The architecture of these calcarenites is markedly different from that of the Claret Conglomerate, the best examples occurring within the central erosional depression of AE-5. In most of this depression alternating fine and medium-grained calcarenites conform a single cross bedded set about 3 m thick, its westward direction being almost perpendicular to the mean palaeocurrents of the Claret Conglomerate (Figs. 9C, 10A). In the westernmost part of the depression, however, this laterally accreted set is almost solely composed of medium-grained calcarenites. A fining-upward arrangement is also evident, with medium-grained calcarenites, which downlap the basal erosional surface of the depression, grading up into fine-grained calcarenites and, eventually, into yellow silty marls (Fig. 10A).

Calcarenites also exist in the Yellowish Soils that filled the western part of the AE-4 central depression. Their arrangement, however, is somewhat more complex than in the AE-5 example, perhaps because they were deposited on the undulating top of the Claret Conglomerate (Supplementary Fig. 6). Other examples of alternating fine and medium-grained calcarenites have been observed directly on top of the Claret Conglomerate in parts of AE-1 and AE-2. Neither exposure is good, as the finer-grained calcarenites are largely covered by vegetation. The medium-grained calcarenites, however, are reasonably well exposed, their fining-up arrangement and low-angle inclined geometry, indicative of lateral accretion, being distinctly perceived (Fig. 10B, C).

4.2. Claret sector

4.2.1. Claret Conglomerate

Only one relatively large outcrop of the Claret Conglomerate occurs in the Claret sector. It is situated around the Claret hamlet, erosively overlying the grey calcarenites and marls of the incised valley fill (Fig. 11A). This outcrop is about 1.5 km long in N — S direction, reaching a maximum thickness of about 4 m in its central part and progressively decreasing to ~1 m in the Palau and Ricos creeks, eventually pinching out a little further to the north and south. In the Claret road section, imbrication in basal conglomerates of the incised valley deposits and cross-stratifications in the Claret Conglomerate indicate WSW-directed palaeocurrents (Pujalte et al., 2022) (Fig. 11A). The close parallelism between the palaeocurrents of these two units can also be clearly perceived in the three-dimensional exposure created by the Palau creek (Fig. 11B), where both units display large-scale trough cross-bedding. In both units, in effect, foresets indicative of west-directed currents occur in the northern and southern margins of the creek (Fig. 11C, E), while cross-cutting scoop shaped erosional surfaces are visible in the N–S oriented outcrop within the creek itself (Fig. 11D). The areal coincidence of the outcrops of both units and their near identical palaeocurrents,

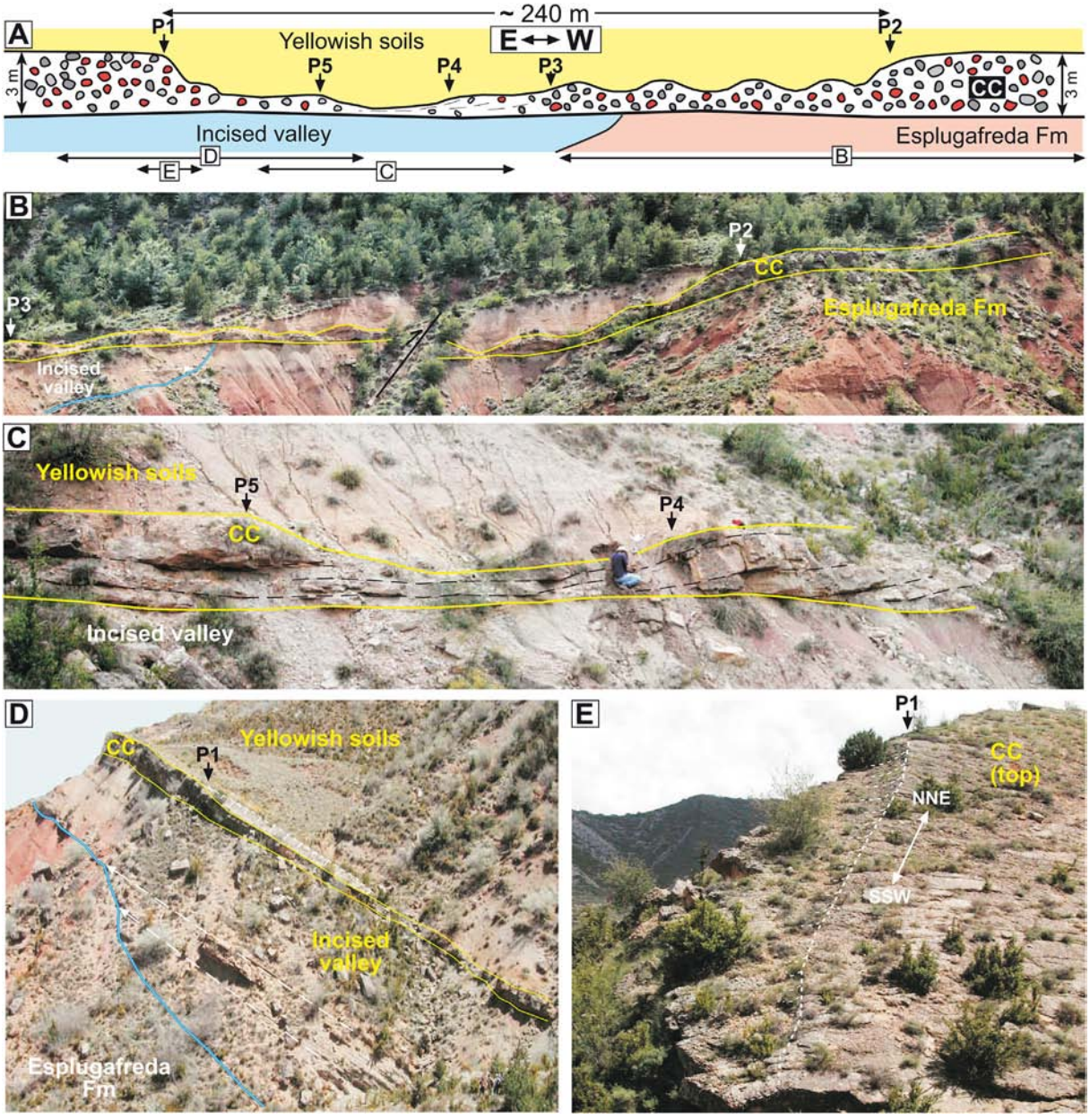

Fig. 8. (A) Simplified sketch of Architectural Ensemble-4 (location in Fig. 3A), with indication of reference points P1 to P5 (CC: Claret Conglomerate). (B–D) Field photos of different segments of the ensemble, all of them looking south. (E) Field photo of the easternmost side of the ensemble's central depression, looking north. Note the rapid thickness reduction of the Claret Conglomerate along line P1. Explanation within the text.

strongly suggest that the incised valley was not entirely fill-up before the onset of the PETM and acted as a trap for the gravels of the Claret Conglomerate.

The remainder outcrops of the Claret Conglomerate in the Claret sector are discontinuous and always overlie directly the Esplugafreda Formation. All of them are of modest dimensions, the largest one, situated on the southern margin of the St Adria valley, being about 170 m wide and up to 2 m thick (Figs. 11A, 12A).

4.2.2. Yellowish Soils

As in Esplugafreda, in the Claret sector the Yellowish Soils are mainly composed of silty marls, which show progressively lighter colours upsection, interspersed with some intercalated calcarenites, of which two types are recognized, channelized and unchannelized, (Fig. 12). The best example of the channelized type, located on the southern margin of the St Adria valley (Fig. 11A), is up to 5 m thick and about 50 m wide. It is mainly composed of 5–15 cm thick calcarenites separated by thin marly interbeds that abut on a concave-up lower surface (Fig. 12B, C). These calcarenites are arranged in several stacked packages, each of them having a low-angle inclination indicative of lateral accretion (Fig. 12C). Other examples of channelized calcarenites, with a similar character and arrangement, were reported by Pujalte et al. (2022) in the Ricos creek and in the Claret road. The unchannelized calcarenites consist of 5–15 cm thick individual tabular beds, most of them with flat erosional bases, intercalated within the silty marls. They are usually poorly exposed, being partly covered by silty marls, which makes it difficult to assess their number and extension. However, several examples can be traced laterally for tens of meters (Fig. 12D).

The large Claret Conglomerate outcrop around the Claret hamlet is almost everywhere overlain by friable silty marls of the Yellowish Soils, the erosion of which has exhumed wide portions of the sharp and nearly flat upper surface of the Claret Conglomerate (Fig. 11C;

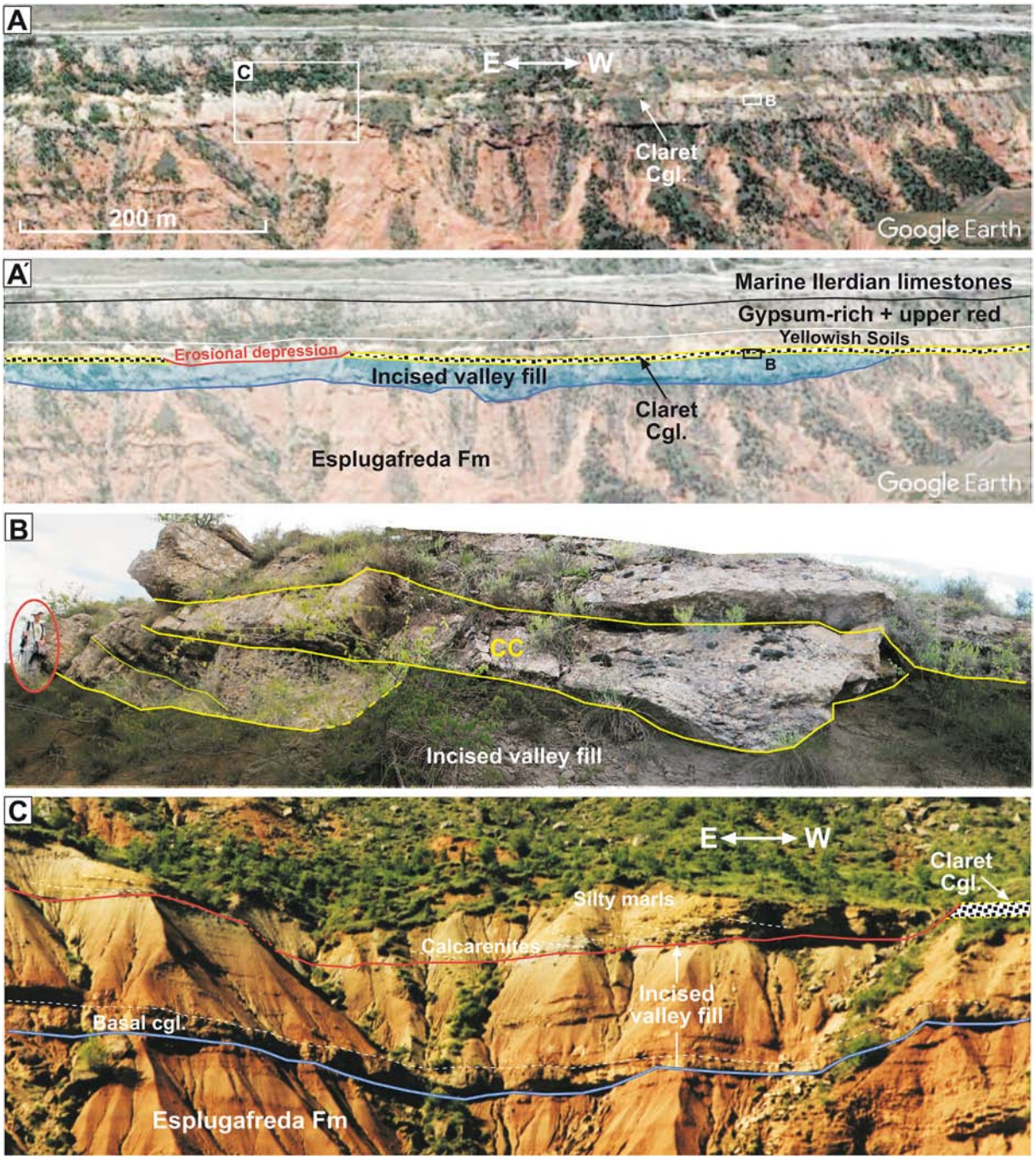

Fig. 9. (A, A') Google Earth/Digital Globe image of the western part of the Esplugafreda outcrop with a superimposed map of the Claret Conglomerate Architectural Ensemble-5 and underlying and overlying units (location in Fig. 3A); note the erosional depression in the central part of the ensemble, in which the Claret Conglomerate has been eroded away. (B) Close up of part of the Claret Conglomerate (CC); encircled geologist on the left gives scale. (C) Enlarged view of part of the ensemble's central depression and of the infilling Yellowish Soil calcarenite channel (see also Fig. 10A for a close-up of part of the channel).

Supplementary Fig. 4C, D). In the St Adria valley, however, the Yellowish Soils indistinctly rest on the Claret Conglomerate or directly on the Esplugafreda Formation (Fig. 12A, D).

5. Discussion

5.1. Setting and climate during pre-PETM times: the Thanetian Esplugafreda Formation

As mentioned above, deposits from the proximal part of the northern margin of the Tremp-Graus Basin were largely removed by erosion after the Ypresian—Oligocene tectonic deformation (Fig. 1B). However, a minor part was preserved in a small outlier near the Coll de Nargo village, about 35 km to the east of Tremp (Supplementary Fig. 1A). In this outlier the former mountain front is girded by Paleocene alluvial fans of comparatively modest dimensions, mostly composed of conglomerates, which grade into red marls with intercalated channels of the Esplugafreda Formation within a few hundreds of metres (Supplementary Fig. 7A). Based on this observation, Schmitz and Pujalte (2007) assumed that the entire northern margin of the Tremp-Graus Basin was flanked by similar alluvial fans in pre-PETM times (Supplementary Fig. 7B).

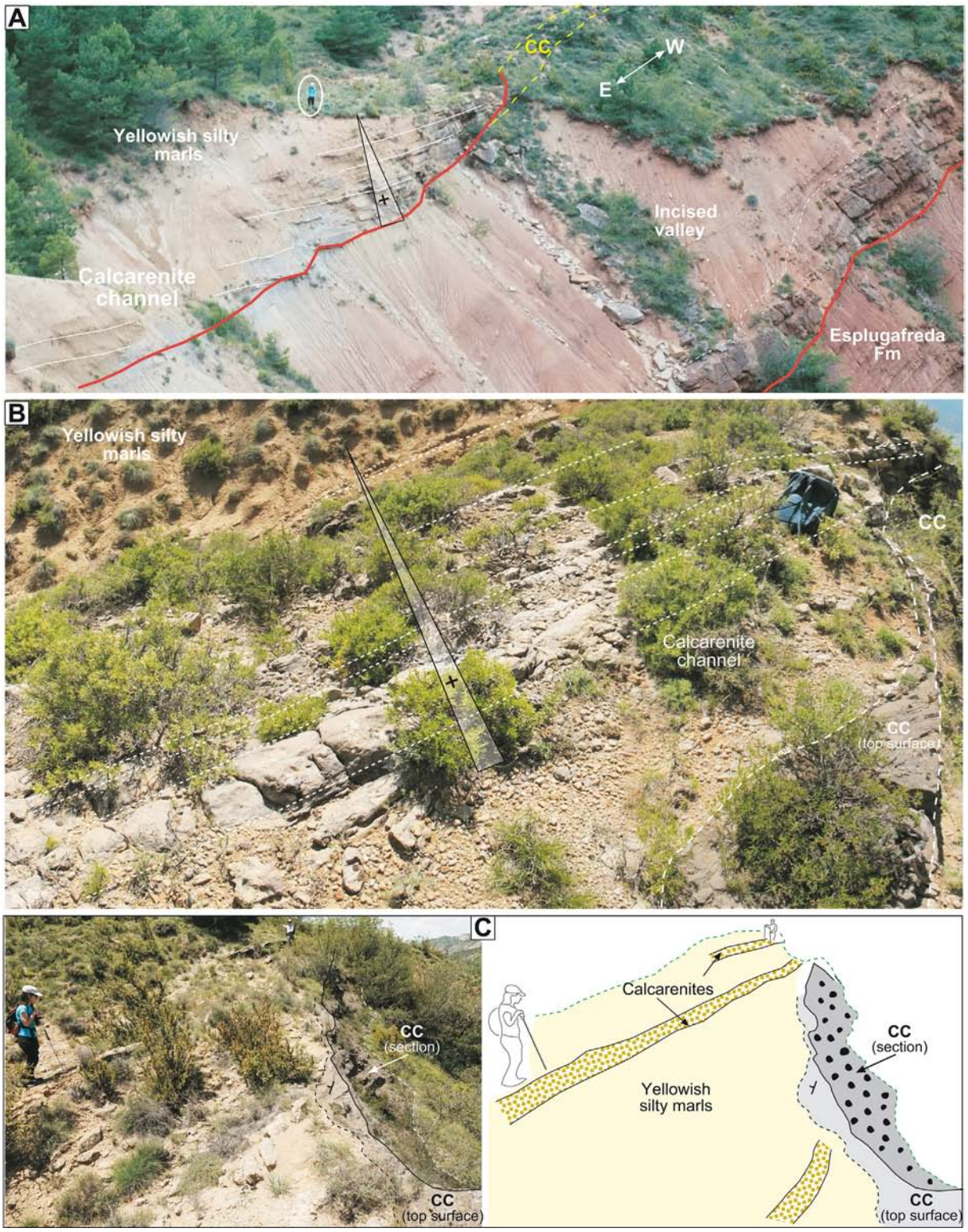

Fig. 10. Examples of laterally accreted calcarenite channels of the Yellowish Soils from the Esplugafreda sector (CC: Claret Conglomerate). (A) Developed within the erosional depression of Architectural Ensemble-5; note the predominance of medium-grained calcarenites in the western part of the depression. (B, C) Developed directly on top of the Claret Conglomerate in Architectural Ensembles-2 and 1, respectively.

The widespread palaeosol carbonate nodules within the red marls of the Esplugafreda Formation provide some climatic information. Carbonate nodules, in effect, form under water deficit conditions. These conditions are generally met in climatic regimes characterized by either perennial arid conditions or a very marked dry season, with a narrow range of annual precipitation from about 100 to 900 mm (Retallack, 2001; He et al., 2015). The co-occurrence of palaeosol carbonate nodules with remains of *Microcodium* (a proxy for Mediterranean climate; Calvet et al., 1991; Kabanov et al., 2008; Pujalte et al., 2019) and, especially, with profuse gypsum deposits, proves that the accumulation of

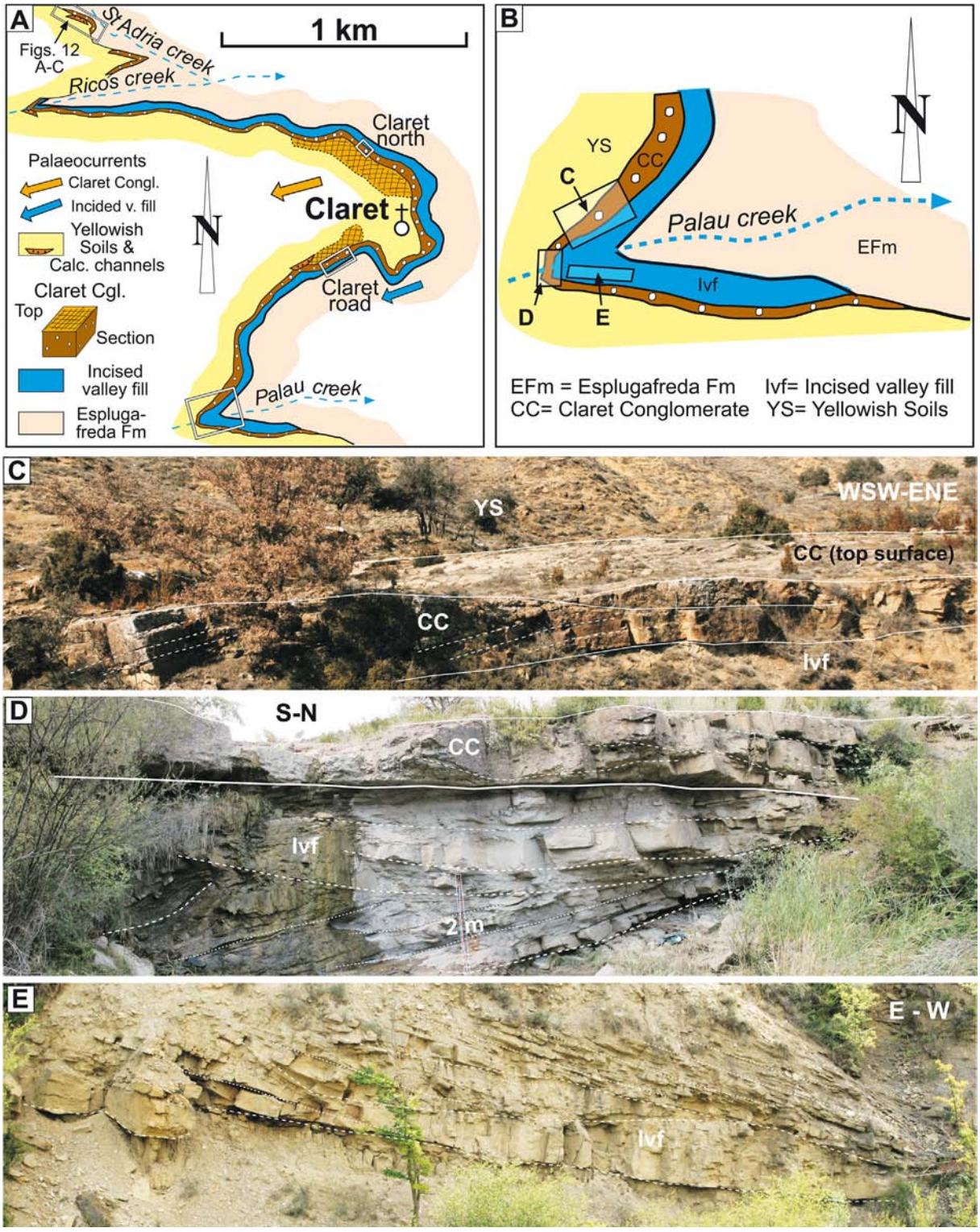

Fig. 11. (A) Outcrop map illustrating the discontinuous character of the Claret Conglomerate in the Claret sector and the near parallel mean palaeocurrent directions of this unit and of the incised valley deposits. (B) Enlarged outcrop map of the Palau creek section with location of the field photos in (C), (D) and (E). Explanation in the text.

the Esplugafreda Formation took place under a prevailing arid/semiarid climate. In addition, Puigdefabregas et al. (1989) reported rootlet surfaces and mud cracks within the channels intercalated in the red marls, which were regarded as evidence of a highly ephemeral alluvial regime.

The present day coastal zone of the Granada province, in southeastern Spain, has geographic and climatic characteristics similar to those of the Tremp-Graus Basin in pre-PETM times, as it is situated at about 37°N latitude, is flanked by mountains and has a semiarid climate. The former is, therefore, a suitable analogue to reconstruct the characteristics and processes on the latter. The Granada coastal zone is drained by a comparatively large river (Guadalfeo) and several smaller ravines, locally named "ramblas", all of which have developed fan deltas at their mouths (Supplementary Fig. 8A). The biggest fan delta, with a radius of ~6 km in its subaerial part, is fed by the Guadalfeo River, which has a drainage area of ~1300 km^2. The ramblas have smaller drainage areas

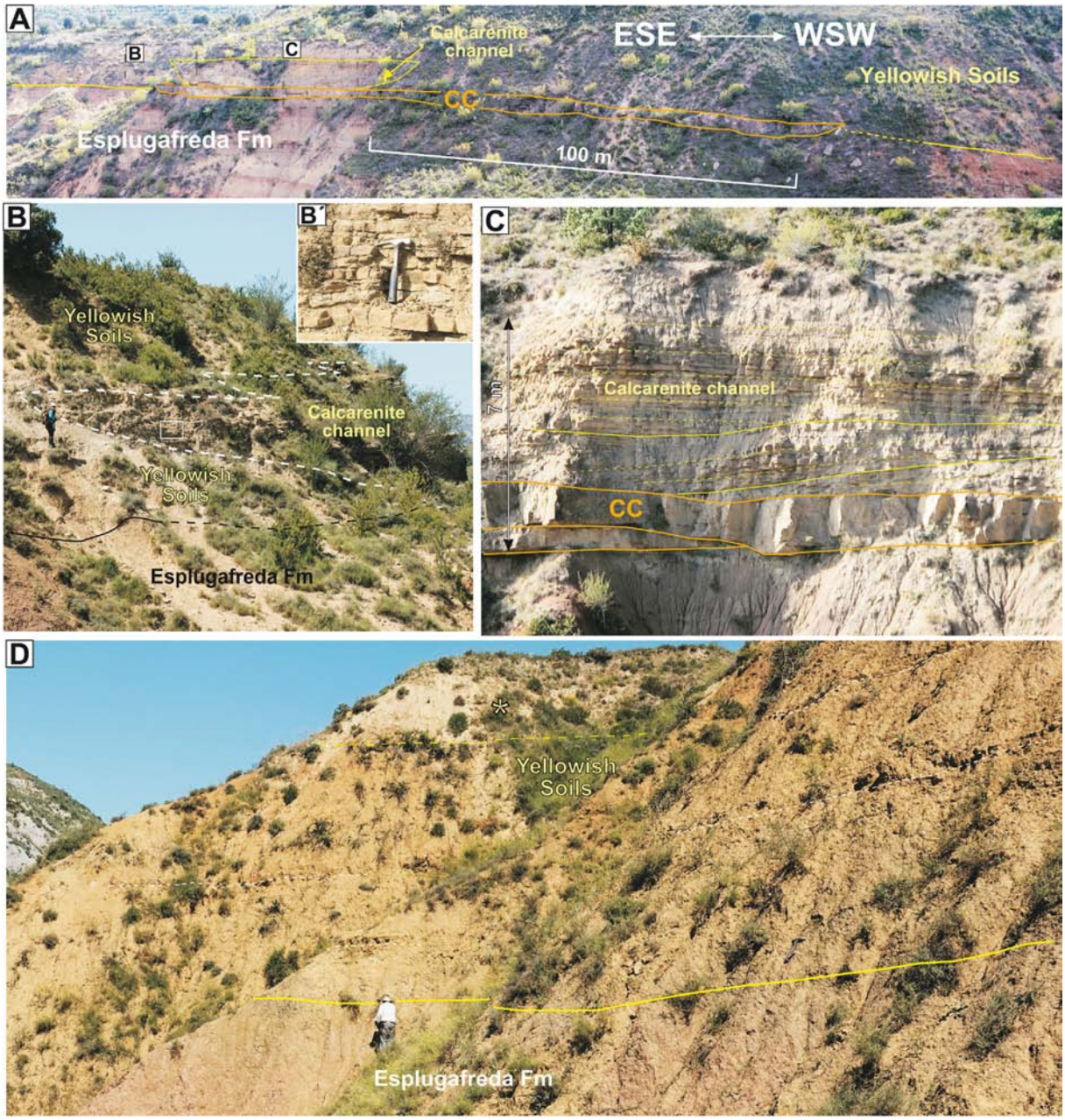

Fig. 12. Field views of PETM units in the St. Adria valley (location in Fig. 11A). (A) The Claret Conglomerate (CC) on the southern (right hand) margin of the valley, locally overlain by a Yellowish Soil calcarenite channel. (B) Eastern pinch-out of the calcarenite channel, with a close-up of its calcarenites (inset). (C) Frontal view of the calcarenite channel illustrating its composite nature. (D) Field view of the Yellowish Soils on the northern (left hand) margin of the valley, with indication of some of their intercalated unchannelized calcarenites; note the light (high chroma) silty marls in the upper part of the unit (indicated by an asterisk).

(≤170 km^2), the subaerial parts of their attached fan deltas being correspondingly smaller, with radii between 1 and 2.5 km (Supplementary Fig. 8B, C). The distal expression of these fan deltas is represented by shallow subaquatic coastal clastic wedges ~1 km wide (Hernández-Molina et al., 1995). The development of these fan deltas was intermittent, mainly occurring during occasional rainstorm episodes. For instance, the subaerial part of the fan delta at the mouth of the Albuñol rambla experienced rapid seaward progradation of up to 270 m after a single, exceptional rainstorm (locally >600 l/m^2) on October 18, 1973 (Capel Molina, 1974; Pujalte et al., 2022).

5.2. Setting of the Claret Conglomerate at the onset of the PETM

As indicated above, the Claret Conglomerate has been interpreted as having been deposited either by braided rivers (Dreyer, 1993; Colombera et al., 2017) or in the vast braidplain of an alluvial megafan (Schmitz and Pujalte, 2007), the latter interpretation entailing that the PETM caused a more radical environmental change than the former. Facies analysis has limited value to weigh the merits of these two alternatives, as lithofacies of gravel-dominated braided rivers and alluvial fans are very similar. However, the architectural features of the Claret Conglomerate described above support the megafan interpretation. On the one hand, rather than the near homogeneous lateral thickness implicit in braided fluvial models (Fig. 2D), the Claret Conglomerate exhibits a large-scale mounded profile at Esplugafreda and nearby sectors, with a convex-up upper surface (Supplementary Fig. 1). Such a profile is typical of the transverse cross-section of alluvial fans, the thickest parts representing their axial zones. On the other hand, the discharge of braided rivers usually increases down current, but the discontinuous character of the Claret Conglomerate in the distal Claret sector implies diminished

discharge, which is typical of alluvial fans. Last, but not least, the features of the five architectural ensembles recognized at Esplugafreda can be satisfactorily explained through comparison with recent small-scale fan-like accumulations.

Indeed, the controls on the architecture of ancient and recent alluvial/fluvial systems are increasingly being investigated with the help of small-scale models created in laboratory flumes (e.g., Strong and Paola, 2006; Reitz and Jerolmack, 2012; Van de Lageweg et al., 2013). In this study, however, we compared the architecture of the Claret Conglomerate with some natural, small-scale fan-like accumulations found during our field studies. The analogues that best match the lateral variability of the Claret Conglomerate in the Esplugafreda sector are those illustrated in Figs. 13—15, all of which developed on near flat, slightly sloping surfaces.

The multiepisodic fan in Fig. 13 was formed next to the trench of an active sand quarry in England. Its innermost zone, here labelled braidplain core (BPc; see Fig. 13 for acronyms), consists of a dense network of braided channels infilled with clean sands (whitish colour in Fig. 13A). Down current from the core different parts can be differentiated, the most prominent being lobe-shaped accumulations of brown-coloured sands (LBb) fed from braided channels (Bch). Similar coloured sands fringing the fan core represent previous lobes (LBa), partly encroached by the core expansion. These lobes have a convex-up upper surface, their flanks sloping to the right and left of the feeding braided channel (Fig. 13B). Intervening zones between lobes contain finer grained sediments and a network of smaller channels (SSd). Lastly, clays (DCl) were accumulated in the most distal part of the fan. The core, braided channels and lobes must have been active during and just after rainy episodes, as they contain the coarsest deposits of the system. After cessation of the rain, diminished runoff flowed preferentially through small channels within the depressed inter-lobe zones (FCh in Fig. 13A).

This model accounts for most of the features of the Claret Conglomerate in the Esplugafreda area. The braidplain core probably existed in the most proximal part of the Tremp-Graus Basin, but is not preserved today (Fig. 1B). However, Architectural Ensembles 1, 2, and 3 can, respectively, be ascribed to different parts situated down current from the core.

Thus, AE-1 can be assigned to either the external part of the braidplain core or to a major braided channel similar to the Scott type of Miall (1978). The predominance of coarse-grained conglomerates in this ensemble is, in effect, a proof of strong currents, the great mobility of the constituent minor channels and interchannel bars being respectively recorded by pervasive cross-cutting erosional surfaces and large-scale cross-strata (Fig. 5B—D). Scour-and-fill relationships, which are common in braided channels, also exist in this ensemble.

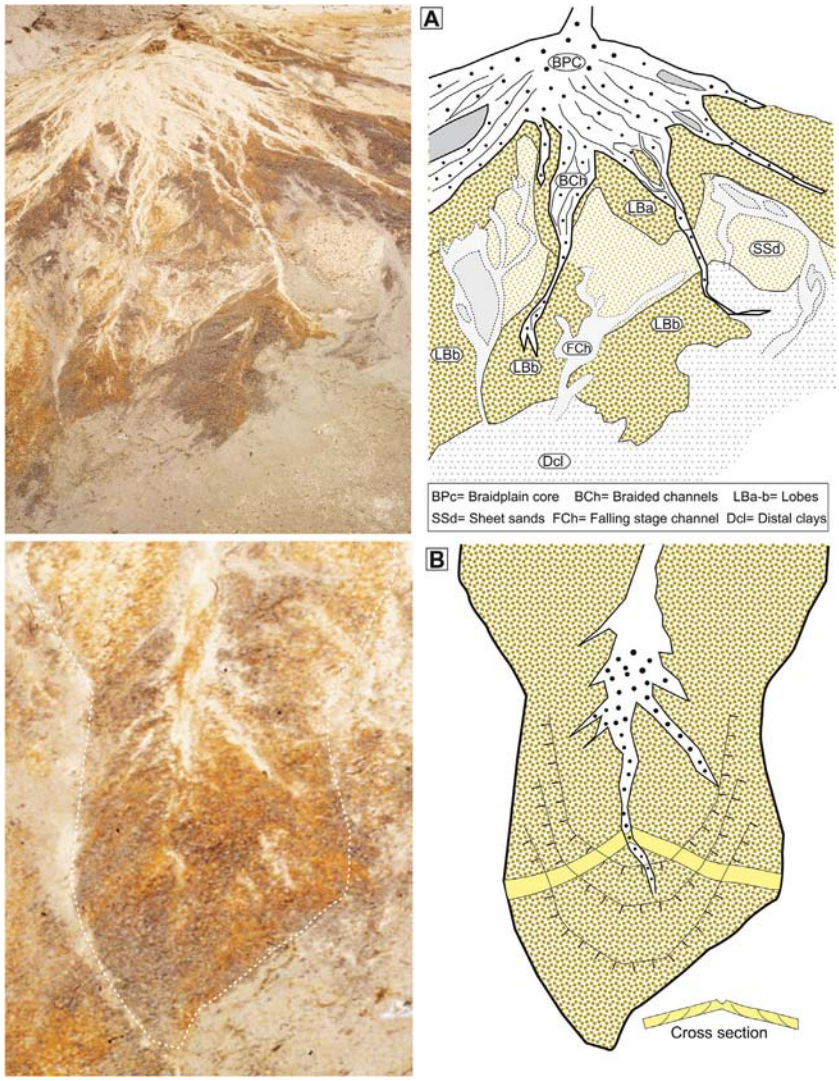

Fig. 13. (A) Field view and interpretative sketch of a recent small-scale alluvial fan developed on the nearly flat floor of a sand quarry in England (height and width: approximately 8 and 4 m). (B) Enlarged view of a lobe-shaped accumulation fed from a braided channel. Explanation within the text.

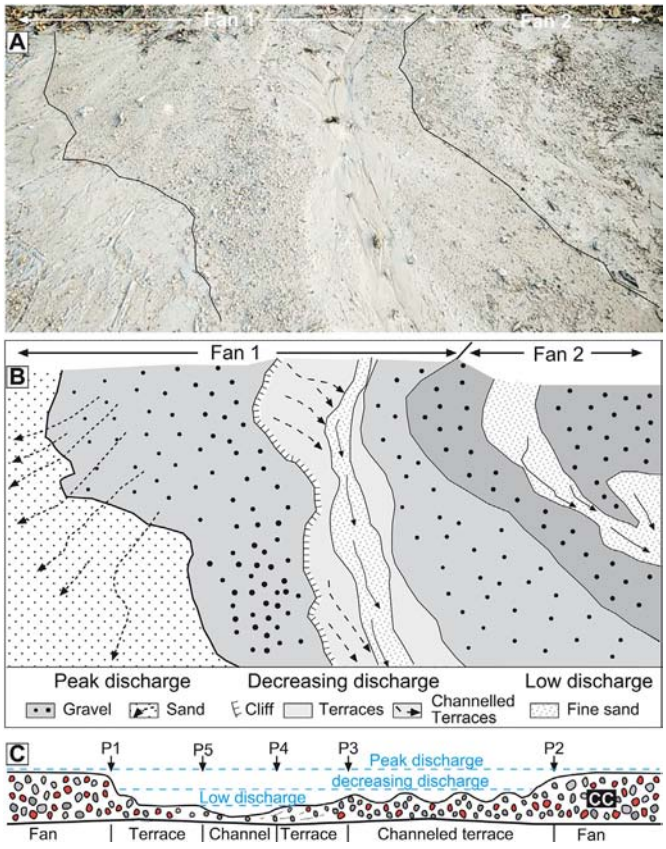

Fig. 14. (A, B) Field view and interpretative sketch of a recent small-scale alluvial fan developed on a nearly flat floor in southeastern Spain (height and width: approximately 2 and 4 m). (C) Interpretation of the Claret Conglomerate (CC) Architectural Ensemble-4 based on this small-scale alluvial fan.

The low-angle inclined strata of AE-2, with near opposite senses of accretion, are best explained by deposition on both flanks of a lobe, its central depression corresponding to the lobe-feeding channel. The variable thicknesses of the strata in the lobe flanks and the coarse-grained nature of their terminal protuberances can respectively be attributed to an intermittent growth of the lobe and to avalanching processes at the toes of the inclined strata. Lastly, the well-defined central channels of AE-3, which cut into ≤2 m thick tabular-shaped conglomerates (Fig. 7A), suggest autogenic compensation processes and most likely represent small channels flowing through inter-lobe depressions (Ventra and Nichols, 2013, and references therein).

The two small-scale fans in Figs. 14 and 15 were originated in eastern Spain after single summer downpours and, consequently, have a simpler configuration. The example in Fig. 14 consists of two coalescent fans, a fact that precluded the full development of a fan-like geometry. However, the radial arrangement of distributary channels is perceptible on the left hand side of fan 1 (Fig. 14A, B). A depression infilled with somewhat finer sediments exists along the axis of this fan, with its lowest zone situated along its central part. This low zone is flanked by terraces, locally crossed by small channels, the terrace on the left being bordered by a small cliff (Fig. 14A, B). An axial depression also exists in fan 2, but not so well developed. The configuration of both small fans was a result of changing discharge after the storm: water spread over the entire fan at peak flow but, as the flow receded, it became restricted to a progressively narrower and deeper depression along the axial zone.

The features of this small-scale model are strikingly similar to those of AE-4 (cf., Figs. 8 and 14A, B), from which it is reasonable to conclude that this ensemble also records a strong variation in water discharge, although not necessarily after one single event. Thus, the parts of the ensemble situated east and west of points P1 and P2 record phase (s) of high discharge. The central depression must have been created during diminishing discharge, the undulating zone between points P2 and P3 satisfactorily comparing to the channelled part of the terrace in Fig. 14, and the segment between points P4 and P5 in Fig. 8C being ascribable to the phase of minimum streamflow.

The small-scale fan in Fig. 15 also records a strong variation in discharge. The fan must have grown, laterally and frontally, at peak discharge, when sedimentation occurred on the entire fan, as recorded by the dry part of the model (whitish, 1 in Fig. 15). With decreasing discharge, flowing water became restricted to discrete channels (light grey, 2 in Fig. 15, still wet) and, after further decrease, to a single channel that became fully entrenched into the fan (dark grey, 3 in Fig. 15).

Two key features of AE-5 can adequately be explained by this model. Thus, the lateral accretion arrangement and abrupt termination of conglomeratic strata (Fig. 9B) are readily attributable to the intermittent lateral growth of the fan during episodes of high discharge, whereas the central depression of the ensemble (Fig. 9A) clearly records current entrenchment at low discharge (Fig. 15).

In summary, the architectural features of the Claret Conglomerate in the Esplugafreda sector are best explained by deposition in a megafan, rather than in separate braided rivers. This implies that the small alluvial fans fringing the northern margin of Tremp-Graus Basin in Thanetian times rapidly expanded and coalesced into the braidplain of a megafan at the onset of the PETM, their deposits mantling most of the northern half of the basin. This interpretation also explains the discontinuous and generally modest dimensions of the Claret Conglomerate outcrops in the Claret sector, which probably represent distal segments of individual lobes. The lens-like shape of the large outcrop around the Claret hamlet suggests a composite package, probably the result of the concentration of lobes along a former, partly buried incised valley.

5.3. Hydroclimatic change at the onset of the PETM

Climate modelling results by Kiehl et al. (2018) indicated that seasonality enhanced in the Pyrenees during the PETM. Both surface air temperature and evaporation increased in summer (June–August), whereas rainfall increased by 50–200%, especially in autumn (October–January), which also led to increased runoff.

To our knowledge, the only specific attempt to quantify the hydrological change induced by the PETM using proxy data from the Tremp-Graus Basin is that of Chen et al. (2018). However, leaving aside that some key data used in their calculation are flawed (see above and Supplementary Fig. 2), it is not clear whether their postulated 1.35 to 14 times increase in water discharge during the PETM refers to individual events or to an augmentation in annual rainfall.

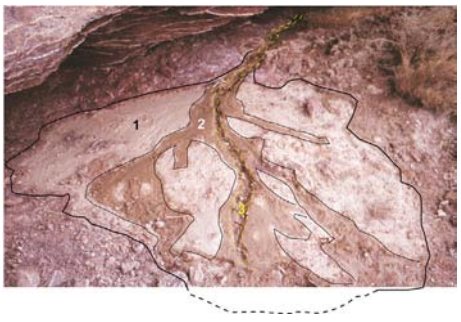

Fig. 15. Field view of a recent small-scale alluvial fan (height and width: approximately 2 and 3 m) developed after a summer storm on a nearly flat surface near Tremp, southern Pyrenees, in which three parts can be differentiated, respectively developed at peak discharge (part 1, whitish), during decreasing discharge (part 2, light grey, still wet), and at low discharge (part 3, dark grey, outlined in yellow in the online version).

Here an alternative approach is used, based on historical and recent records of floods and meteorological data from mid-latitude Spain during the last century (Supplementary Fig. 9). The rationale for this approach is that, although global boundary conditions were different in PETM times, both the palaeogeographic and palaeoclimatic characteristics of the Tremp-Graus Basin were similar to those of today's southeastern Spain, as discussed above. Therefore, historical and recent meteorological records from Spain may provide some clues about the hydrological changes in the Tremp-Graus Basin at the onset of the PETM, assuming that the anthropogenic warming and the PETM are comparable events.

The Spanish records demonstrate that from 1916 to 2019 the number of floods caused by exceptional rainfall events has increased steadily (see Supplementary Fig. 9A for actual data and plot). This trend can also be observed in the floods of rivers debouching into the Mediterranean in SE Spain ("SE coastal basins" in Supplementary Fig. 9A). In the Guadalfeo River, for example, five large floods were recorded between the years 835 and 1985 (a return period of 230 years), and another five between 1917 and 1973 (a return period of 56 years) (Rodríguez-Martínez and Mesa-Garrido, 2016. The effect of these recent floods on the fan deltas is minimized by the construction of dams and other corrective measures in the river courses. However, as mentioned above, the fan delta attached to the Albuñol rambla, in which no dam exists, prograded up to 270 m after a single rainstorm in 1973. Interestingly, historical meteorological data show that out of 27 exceptional rainfall events in the Mediterranean Spanish SE coastal basins between 1916 and 2019, 20 occurred in October and November and another four in September; only one occurred in January and two in February. This compares well with the palaeoclimatic conditions modelled for the PETM Tremp-Graus Basin, which deduced increased rainfall and runoff in autumn (Kiehl et al., 2018).

Yet, data from four meteorological stations from coastal Mediterranean Spanish cities demonstrate that, in the last eighty years, the cumulative amount of rain during successive quinquennia, although variable, has not changed significantly (Supplementary Fig. 9C). Consequently, assuming that the recent hydrological changes in Spain are comparable to those during the PETM onset, it is reasonable to conclude that the single most important cause of the expansion of the Claret Conglomerate was a strong enhancement of seasonality, with a concomitant increase in the frequency and intensity of rainstorms in autumn, but without a significant variation in the volume of averaged total annual precipitation.

5.4. Setting and hydroclimate during the core of the PETM: The Yellowish Soils

The lateral accretion and fining upward arrangement of the calcarenites intercalated in the Yellowish Soils at Esplugafreda are clear proof of accumulation on point bars of meandering rivers. The regular alternation of very fine- and medium-grained calcarenites in these point bars suggests a rather stable fluvial regime (Fig. 10). Medium-grained calcarenites, however, are dominant in the westernmost part of the point bar encased within the central depression of AE-5 (Fig. 10A). Likely, the lateral growth of the point bar progressively infilled the depression, narrowing the channel cross-section and increasing flow velocity, which hindered the deposition of fine-grained load. The multistorey character of the channelized calcarenites included in the Yellowish Soils of the Claret sector, together with the lateral accretion of their stacked packages, are indicative of fluvial meander belts. The unchannelized calcarenites, on the other hand, most likely record crevasse splay deposits. The high proportion of fine-grained sediments in the Yellowish Soils, both at Esplugafreda and Claret, requires extensive floodplains. This fact provides additional evidence for a meandering fluvial system, since abundance of suspended load and cohesive banks favours meandering courses.

The abundant small-sized carbonate nodules of the Yellowish Soils suggest perennial or seasonal (semi)arid conditions, since that kind of nodule is only formed under water deficit conditions (Retallack, 2001). The conspicuous absence of *Microcodium* and gypsum in the Yellowish Soils attests to a generally more humid (or less arid) climate than in pre-PETM times. Furthermore, clastic sedimentation rates during the accumulation of the Yellowish Soils increased 5–10 fold, an increase also observed in coeval marine sections of the Pyrenees. This increase indicates a high yield of detritus in the river discharge and deep physical erosion of the landscape, which suggests long and dry summers leading to the absence of a dense, protective vegetation cover (Schmitz et al., 2001; Schmitz and Pujalte, 2003). Interestingly, the carbonate nodules of the Yellowish Soils are homogeneously dispersed throughout the silty marls in the two studied zones (Fig. 2A, B), a distribution typical of cumulate soil profiles (in the sense of Wright and Marriott, 1996, and Kraus, 1999). These soils develop by (near) steady aggradation through frequent increments of sediments, so that the upper part of their profile is buried and reorganized by processes occurring at deeper levels (Wright and Marriot, 1996, p. 908). Carbonate nodules typically form in the lower horizon of the soil profile, the so-called calcic horizon or Bk (Retallack, 2001). Therefore, their occurrence throughout the whole thickness of the Yellowish Soils is clear proof of the destruction, through reworking, of the upper palaeosol horizons. Additional increments of sediments eventually placed the Bk horizons below the zone of active pedogenesis, which accounts for their preservation and explains the small size of the nodules. These processes necessarily entail frequent inundation of the floodplains represented by the silty marls of the Yellowish Soils, but the absence of coarse-grained deposits demonstrates a drastic diminution of the high magnitude floods inferred for the Claret Conglomerate. Taken together, these facts indicate recurrent but rather tranquil stream flows and, consequently, a more evenly distributed rain during the wet season. Finally, the progressively higher chroma of the silty marl palaeosols towards the upper part of the unit (Supplementary Fig. 5) suggests a trend to increasingly drier conditions (cf., Armengolt et al., 2019).

The generally sharp boundary between the Claret Conglomerate and the Yellowish Soils (Supplementary Fig. 4) might be interpreted as an abrupt transition between their respective hydroclimate states. However, the transition from the onset to the core phases of the PETM in $\delta^{13}C$ isotopic profiles is gradual (e.g., Fig. 2A; see also Zachos et al., 2008), which should have resulted in a similarly progressive sedimentary change. Evidence for such a gradual change is provided by the central depressions in architectural ensembles 4 and 5 of the Claret Conglomerate, which, as discussed above, are attributable to a progressive reduction in flow magnitude (Figs. 14, 15). In effect, avulsion processes are particularly common in low gradient alluvial fans (Gole and Chitale, 1996) and so, at different times, sediments would accumulate on most parts of the Claret Conglomerate. However, the decrease of high magnitude flows would reduce avulsion frequency, the diminished flows becoming restricted, and eventually entrenched, along specific tracts of the former megafan, creating depressed zones in its upper part. The occupation of both central depressions by meandering rivers most likely culminated the transition between the sedimentary and hydroclimatic regimes represented by the Claret Conglomerate and the Yellowish Soils.

5.5. Setting and hydroclimate during the recovery of the PETM: the Gypsum-rich Unit

As previously noted by several authors (e. g., Schmitz and Pujalte, 2003; Domingo et al., 2009; Pujalte et al., 2022), the climate became quite arid in the Tremp-Graus Basin during the recovery phase of the PETM, an aridification process heralded by the high chroma palaeosols of the upper part of the Yellowish Soils. In effect, in addition to its telltale gypsum abundance, a distinctive feature of the Gypsum-rich Unit is the complete absence of carbonate nodules, which suggests that during the recovery phase of the PETM annual precipitation was less than 100 mm (cf., Retallack, 2001). Furthermore, the absence of

conglomerates and calcarenites within the unit demonstrates that the currents resulting from occasional rains were only capable of transporting silts and clays (Fig. 3C), and must therefore have been of reduced volume and strength. Lastly, the accumulation of alabastrine gypsum in the Claret area is proof that the eventual flows reaching the Claret area evaporated in saline lakes (Fig. 3D).

6. Conclusions

The notion that the PETM induced an important change in hydroclimate is far from new. The data here presented confirm that change, but also show that in the mid-latitude terrestrial Tremp-Graus Basin the hydroclimate varied in parallel with the three phases of the hyperthermal event, profoundly altering depositional conditions as the CO_2 content in the atmosphere varied.

In this basin, in effect, an arid/semiarid climate persisted during Thanetian times, when the mountainous northern margin of the basin was fringed by alluvial fans of comparatively small dimensions. The rapid addition of CO_2 during the onset of the PETM prompted an enhancement of seasonality, inducing frequent rainstorms and high magnitude floods in autumn. This hydroclimate forced a rapid expansion of the previous marginal alluvial fans, which coalesced to create an extensive conglomeratic braidplain in the proximal part of a megafan that mantled the northern half of the basin, represented by the Claret Conglomerate.

During the core of the PETM the percentage of CO_2 in the atmosphere was higher, but remained more or less stable. Seasonality became less contrasted, still with long, dry summers but without, or with few, high magnitude floods and with the rain more equally distributed throughout the wet season. As a result, meandering rivers with extensive floodplains encroached onto the entire basin. Inundations of the flood plains were frequent in the wet season, the concomitant sedimentary flux causing their aggradation. The absence of a dense vegetation cover led to deep physical erosion of the landscape and high fluvial sediment yield, which induced a significant increase in sedimentation rate relative to pre-PETM times, an increase also recorded in marine settings of the Pyrenees. Total annual rain, however, diminished towards the end of this phase, initiating a trend that culminated in an arid hydroclimate during the recovery of the PETM, when saline lakes developed in the central part of the basin.

During the PETM the Tremp-Graus Basin was situated at ~35°N palaeolatitude, between the dry subtropical zone to the south and the subhumid temperate climate zone to the north, a transitional area especially sensitive to global climate changes. This specific latitudinal location most probably enhanced the hydroclimate variations during the successive phases of the hyperthermal event.

The PETM is widely acknowledged as an ancient analogue of the ongoing anthropogenic warming, which seems to be in its onset phase. Continental outcrops like the unique Pyrenees sections studied herein provide the most informative records of the succession of climate change phases during the PETM. If the current rates of CO_2 emissions continue unabated, a sequence of hydroclimatic and environmental changes similar to those registered in the Tremp-Graus Basin can be expected in mid-latitude terrestrial basins and coastal plains adjacent to, and fed from, nearby mountainous areas.

Declaration of competing interest

The authors declare that they have no competing financial interests or personal relationships that could have influenced the research reported in this paper.

Acknowledgements

Research by AP and VP was supported by MINECO/MCI/FEDER-UE projects PID2019-105670GB-I00/AEI/10.13039/501100011033 of the Spanish Government and by the Consolidated Research Group IT930-16 of the Basque Government. Research by BS was supported by a Linné Grant from the Swedish Research Council. Comments by two anonymous reviewers and editor Catherine Chagué helped to improve the original manuscript.

Appendix A. Supplementary data

Supplementary data to this article can be found online at https://doi.org/10.1016/j.sedgeo.2022.106155.

References

Alley, R.B., 2016. A heated mirror for climate change. Science 352, 151–152.

Ardèvol, L., Klimowitz, J., Malagón, J., Nagtegaal, P.J.C., 2000. Depositional sequence response to foreland deformation in the Upper Cretaceous of the Southern Pyrenees, Spain. American Association of Petroleum Geologists Bulletin 84, 566–587.

Armengolt, O., Liutkus-Pierce, C.M., Takashita-Bynum, K.K., 2019. Using paleosol chroma and mineralogy to track climate and environmental changes at Loperot, Kenya during the early Miocene. GSA Abstracts with Programs 51, 3. https://doi.org/10.1130/abs/2019SE-327014.

Armitage, J.J., Duller, R.A., Whittaker, A.C., Allen, P.A., 2011. Transformation of tectonic and climatic signals from source to sedimentary archive. Nature Geoscience 4, 231–235.

Armitage, J.J., Dunkley Jones, T., Duller, R.A., Whittaker, A.C., Allen, P.A., 2013. Temporal buffering of climate-driven sediment flux cycles by transient catchment response. Earth and Planetary Science Letters 369–370, 200–210.

Baceta, J., Pujalte, V., Wright, V.P., Schmitz, B., 2011. Carbonate platform models, sealevel changes and extreme climatic events during the Paleocene-early Eocene greenhouse interval: a basin-platform-coastal plain transect across the southern Pyrenean basin. In: Arenas, C., Pomar, L., Colombo, F. (Eds.), Pre-Meeting Field Trips Guidebook, 28th IAS Meeting, Zaragoza. Geo-Guíasvol. 7, pp. 151–198.

Burbank, D.W., Vergés, J., Muñoz, J.A., Bentham, P., 1992. Coeval hindward- and forward-imbricating thrusting in the south-central Pyrenees, Spain: timing and rates of shortening and deposition. Geological Society of America Bulletin 104, 3–17.

Calvet, F., Wright, V.P., Gimenez, J., 1991. *Microcodium*: descripción y origen: implicaciones paleogeográficas, paleoclimatológicas y paleogeomorfológicas. Actas Ier Congreso del Grupo Español del Terciario, Vic, Spain, pp. 50–51 (in Spanish).

Capel Molina, J., 1974. Génesis de las inundaciones de Octubre de 1973 en el Sureste de la Península Ibérica. Cuadernos Geográficos de la Universidad de Granada4 pp. 140–166 (in Spanish).

Carmichael, M.J., Inglis, G.N., Badger, M.P.S., Naafs, D.A., Behrooza, L., Remmelzwaal, S., Monteiro, F.M., Rohrssen, M., Farnsworth, A., Buss, H.L., Dickson, A.J., Valdes, P.J., Lunt, D.J., Pancost, R.D., 2017. Hydrological and associated biogeochemical consequences of rapid global warming during the Paleocene-Eocene thermal Maximum. Global and Planetary Change 157, 114–138.

Carmichael, M.J., Pancost, R.D., Lunt, D.J., 2018. Changes in the occurrence of extreme precipitation events at the Paleocene–Eocene thermal maximum. Earth and Planetary Science Letters 501, 24–36.

Cecil, C.B., Dulong, F.T., 2003. Precipitation models for sediment supply in warm climates. In: Cecil, C.B., Edgar, N.T. (Eds.), Climate Controls on Stratigraphy. SEPM Special Publicationvol. 77, pp. 21–27.

Centore, P., 2013. Conversions between the Munsell and sRGB colour systems. Colour tools for painters https://www.munsellcolourscienceforpainters.com/. (Accessed 30 March 2022).

Chanvry, E., Deschamps, R., Joseph, P., Puigdefàbregas, C., Poyatos-Moré, M., Serra-Kiel, J., Garcia, D., Teinturier, S., 2018. The influence of intrabasinal tectonics in the stratigraphic evolution of piggyback basin fills: towards a model from the Tremp-Graus-Ainsa Basin (South-Pyrenean Zone, Spain). Sedimentary Geology 377, 34–62.

Chen, Ch., Guerit, L., Foreman, B.Z., Hassenruck-Gudipati, H.J., Adatte, Th., Honegger, L., Perret, M., Sluijs, A., Castelltort, S., 2018. Estimating regional flood discharge during Palaeocene-Eocene global warming. Scientific Reports 8, 13391.

Colombera, L., Arévalo, O.J., Mountney, N.P., 2017. Fluvial-system response to climate change: the Paleocene-Eocene Tremp Group, Pyrenees, Spain. Global and Planetary Change 157, 1–17.

Cuevas, J.L., 1992. Estratigrafía del "Garumniense" de la Conca de Tremp, Prepirineo de Lérida. Acta Geologica Hispánica 27, 95–108 (in Spanish).

Domingo, L., López-Martínez, N., Leng, M.J., Grimes, S.T., 2009. The Paleocene–Eocene Thermal Maximum record in the organic matter of the Claret and Tendruy continental sections (South-central Pyrenees, Lleida, Spain). Earth and Planetary Science Letters 281, 226–237.

Dreyer, T., 1993. Quantified fluvial architecture in ephemeral stream deposits of the Esplugafreda Formation (Paleocene), Tremp-Graus Basin, northern Spain. In: Marzo, M., Puigdefábregas, C. (Eds.), Alluvial Sedimentation. IAS Special Publicationvol. 17, pp. 337–362.

Eppes, M.C., Johnson, B.G., 2022. Chapter 3.24: describing soils in the field: a manual for geomorphologist. In: Shroder, J.F. (Ed.), Treatise on Geomorphology, 2nd ed. Elsevier, Amsterdam, pp. 450–479.

Fernández, O., Muñoz, J.A., Arbués, P., Falivene, O., 2012. 3D structure and evolution of an oblique system of relaying folds: the Ainsa basin (Spanish Pyrenees). Journal of the Geological Society 169, 545–559.

Foreman, B.Z., 2014. Climate-driven generation of a fluvial sheet sand body at the Paleocene-Eocene boundary in north-west Wyoming (USA). Basin Research 26, 225–241.
Foreman, B.Z., Heller, P.L., Clementz, M.T., 2012. Fluvial response to abrupt global warming at the Palaeocene/Eocene boundary. Nature 491, 92–95.
García Veigas, J., 1997. First continental evaporitic phase in the South Pyrenean central area: Tremp gypsum (Garumn facies, upper Paleocene; allochtonous zone). In: Busson, G., Schreiber, B.Ch. (Eds.), Sedimentary Deposition in Rift and Foreland Basins in France and Spain (Paleogene and Lower Neogene). Columbia University Press, Columbia, pp. 335–342.
Gibson, T.G., Bybell, L.M., Mason, D.B., 2000. Stratigraphic and climatic implications of clay mineral changes around the Paleocene/Eocene boundary of the northeastern US margin. Sedimentary Geology 134, 65–92.
Gole, C.V., Chitale, S.V., 1996. Inland delta building activity of Kosi River. Journal of Hydraulic Engineering 92, 111–126.
He, W., He, H., Zhu, M., 2015. Calcium nodules as a proxy for Quaternary paleoclimate change on China's Loess Plateau. PLoS One 10, e0143928. https://doi.org/10.1371/journal.pone.0143928.
Heller, P.L., Paola, C., 1989. The paradox of Lower Cretaceous gravels and the initiation of thrusting in the Sevier orogenic belt, United States Western Interior. Geological Society of America Bulletin 101, 864–875.
Hernández-Molina, F.J., Somoza, L., Vázquez, J.T., Rey, J., 1995. Estructuración de los prismas litorales del Cabo de Gata: respuesta a los cambios climático-eustáticos holocenos. Geogaceta 18, 79–82 (in Spanish).
Jiang, J., Hu, X., Li, J., BouDagher-Fadel, M., Garzanti, E., 2021. Discovery of the Paleocene-Eocene Thermal Maximum in shallow-marine sediments of the Xigaze forearc basin, Tibet: a record of enhanced extreme precipitation and siliciclastic sediment flux. Palaeogeography Palaeoclimatology Palaeoecology 562, 110095. https://doi.org/10.1016/j.palaeo.2020.110095.
John, C.M., Bohaty, S.M., Zachos, J.C., Sluijs, A., Gibbs, S., Brinkhuis, H., Bralower, T.J., 2008. North American continental margin records of the Paleocene–Eocene thermal maximum: implications for global carbon and hydrological cycling. Paleoceanography 23, PA2217. https://doi.org/10.1029/2007PA001465.
Kabanov, P., Anadón, P., Krumbein, W.E., 2008. *Microcodium*: an extensive review and a proposed non-rhizogenic biologically induced origin for its formation. Sedimentary Geology 205, 79–99.
Kiehl, J.T., Shields, C.A., Snyder, M.A., Zachos, J.C., Rothstein, M., 2018. Greenhouse- and orbital-forced climate extremes during the early Eocene. Philosophical Transactions A 376, 20170085. https://doi.org/10.1098/rsta.2017.0085.
Klappa, C.F., 1978. Biolithogenesis of *Microcodium*: elucidation. Sedimentology 25, 489–522.
Klappa, C.F., 1980. Rhizoliths in terrestrial carbonates: classification, recognition, genesis and significance. Sedimentology 27, 613–629.
Košir, A., 2004. *Microcodium* revisited: root calcification products of terrestrial plants on carbonate-rich substrates. Journal of Sedimentary Research 74, 845–857.
Kraus, M.J., 1999. Paleosols in clastic sedimentary rocks: their geologic applications. Earth-Science Reviews 47, 41–70.
Lunt, D.J., Huber, M., Baatsen, M.L.J., Caballero, R., DeConto, R., Donnadieu, Y., Evans, D., Feng, R., Foster, G., Gasson, E., von der Heydt, A.S., Hollis, C.J., Kirtland Turner, S., Korty, R.L., Kozdon, R., Krishan, S., Ladant, J.B., Langebroek, P., Lear, C.H., LeGrande, A.N., Littler, K., Marwick, P., Otto-Bliesner, B., Pearson, P., Poulsen, C., Salzmann, U., Shields, C., Snell, K., Starz, M., Super, J., Tabour, C., Tierney, J., Tourte, G.J.L., Upchurch, G.R., Wade, B., Wing, S.L., Winguth, A.M.E., Wright, N., Zachos, J.C., Zeebe, R., 2017. The DeepMIP contribution to PMIP4: experimental design for model simulations of the EECO, PETM, and pre-PETM (version 1.0). Geoscientific Model Development 10, 889–901.
Manners, H.R., Grimes, S.T., Sutton, P.A., Domingo, L., Leng, M.J., Twitchett, R.J., Hart, M.B., Dunkley Jones, T., Pancost, R.D., Duller, R., Lopez-Martinez, N., 2013. Magnitude and profile of organic carbon isotope records from the Paleocene–EoceneThermal Maximum: evidence from northern Spain. Earth and Planetary Science Letters 376, 220–230.
McInerney, F.A., Wing, S.L., 2011. The Paleocene Eocene Thermal Maximum: a perturbation of carbon cycle, climate, and biosphere with implications for the future. Annual Review of Earth and Planetary Sciences 39, 489–516.
Miall, A.D., 1978. Lithofacies types and vertical profile models in braided river deposits: a summary. In: Miall, A.D. (Ed.), Fluvial Sedimentology. Canadian Society of Petroleum Geologists Memoirvol. 5, pp. 597–604.
Munsell Color, 2009. Geological Rock-Color Chart with Genuine Munsell Color Chips. Munsell Color, Grand Rapis, MI (9 pp.).
Pancost, R.D., 2017. Climate change narratives. Nature Geosciences 10, 466–468.
Plaziat, J.C., 1981. Late Cretaceous to Late Eocene paleogeographic evolution of southwest Europe. Palaeogeography Palaeoclimatology Palaeoecology 36, 263–320.
Plink-Björklund, P., Birgeneier, L., Jones, E., 2014. Extremely bad early Eocene weather: evidence for extreme precipitation from rived deposits. Rendiconti Online della Società Geologica Italiana 31, 175–176.
Puigdefabregas, C., Nijman, W., Muñoz, J.A., 1989. Alluvial Deposits of the Successive Foreland Basin Stages and their Relation to the Pyrenean Thrust Sequences. Guidebook Series of the 4th International Conference on Fluvial Sedimentology. Publicacions del Servei Geològic de Catalunya, Barcelona, Spain (176 pp.).
Pujalte, V., Schmitz, B., 2005. Revisión de la estratigrafía del Grupo Tremp ("Garumniense", Cuenca de Tremp-Graus, Pirineos meridionales). Geogaceta 38, 79–82 (in Spanish).
Pujalte, V., Schmitz, B., 2019. Record of the Paleocene–Eocene Thermal Maximum in the southern and western Pyrenees. In: Quesada, C., Oliveira, J.T. (Eds.), The Geology of Iberia: A Geodynamic Approach. Springer Nature, Switzerland AG, pp. 13–17 https://doi.org/10.1007/978-3-030-11190-8_2.
Pujalte, V., Schmitz, B., Baceta, J.I., 2014. Sea-level changes across the Paleocene–Eocene interval in the Spanish Pyrenees, and their possible relationship with North Atlantic magmatism. Palaeogeography Palaeoclimatology Palaeoecology 393, 45–60.
Pujalte, V., Baceta, J.I., Schmitz, B., 2015. A massive input of coarse-grained siliciclastics in the Pyrenean Basin during the PETM: the missing ingredient in a coeval abrupt change in hydrological regime. Climate of the Past 11, 1653–1672.
Pujalte, V., Robador, A., Payros, A., Samsó, J.M., 2016. A siliciclastic braid delta within a lower Paleogene carbonate platform (Ordesa-Monte Perdido National Park, southern Pyrenees, Spain): record of the Paleocene–Eocene Thermal Maximum perturbation. Palaeogeography Palaeoclimatology Palaeoecology 459, 453–470.
Pujalte, V., Monechi, S., Ortiz, S., Orue-Etxebarria, X., Rodríguez-Tovar, F., Schmitz, B., 2019. *Microcodium*-rich turbidites in hemipelagic sediments during the Paleocene-Eocene Thermal Maximum: evidence for extreme precipitation events in a Mediterranean climate (Río Gor section, southern Spain). Global and Planetary Change 178, 153–167.
Pujalte, V., Schmitz, B., Payros, A., 2022. A rapid sedimentary response to the Paleocene-Eocene thermal Maximum hydrological change: new data from alluvial units of the Tremp-Graus Basin (Spanish Pyrenees). Palaeogeography Palaeoclimatology Palaeoecology 589, 110818. https://doi.org/10.1016/j.palaeo.2021.110818.
Reitz, M., Jerolmack, D.J., 2012. Experimental alluvial fan evolution: channel dynamics, slope controls, and shoreline growth. Journal of Geophysical Research - Earth Surface 117 (F2), F02021. https://doi.org/10.1029/2011JF002261.
Retallack, G.J., 2001. Soils of the Past. Blackwell Science, Oxford, UK (404 pp.).
Rodríguez-Martínez, F., Mesa-Garrido, M.A., 2016. Inundaciones históricas y desertificación en el sector central de la vertiente surmediterránea andaluza (Málaga y Granada). In: Vera-Rebollo, J.F., Olcina, J., Hernández-Hernández, M. (Eds.), Libro Homenaje al Profesor Alfredo Morales Gil. Publicaciones de la Universidad de Alicante, Alicante, Spain, pp. 1023–1048 (in Spanish).
Rosell, J., Linares, R., Lompart, C., 2001. El "Garumniense" prepirenaico. Revista de la Sociedad Geológica de España 14, 47–56 (in Spanish).
Schmitz, B., Pujalte, V., 2003. Sea-level, humidity, and land-erosion records across the initial Eocene thermal maximum from a continental-marine transect in northern Spain. Geology 31, 689–692.
Schmitz, B., Pujalte, V., 2007. Abrupt increase in seasonal extreme precipitation at the Paleocene-Eocene boundary. Geology 35, 215–218.
Schmitz, B., Pujalte, V., Núñez-Betelu, K., 2001. Climate and sea-level perturbations during the Incipient Eocene thermal Maximum: evidence from siliciclastic units in the Basque Basin (Ermua, Zumaia and Trabakua Pass), northern Spain. Palaeogeography Palaeoclimatology Palaeoecology 165, 299–320.
Serra-Kiel, J., Canudo, J.I., Dinares, J., Molina, E., Ortiz, N., Pascual, J.O., Samso, J.M., Tosquella, J., 1994. Cronoestratigrafía de los sedimentos marinos del Terciario inferior de la Cuenca de Graus-Tremp (Zona Central Surpirenaica). Revista de la Sociedad Geológica de España 7, 273–297 (in Spanish).
Slotnick, B.S., Dickens, G.R., Nicolo, M.J., Hollis, C.J., Crampton, J.S., Zachos, J.C., Sluijs, A., 2012. Large-amplitude variations in carbon cycling and terrestrial weathering during the Latest Paleocene and Earliest Eocene: the record at Mead Stream, New Zealand. Journal of Geology 120, 487–505.
Sluijs, A., Bowen, G.J., Brinkhuis, H.L., Lourens, J., Thomas, E., 2007. The Palaeocene–Eocene Thermal Maximum super greenhouse: biotic and geochemical signatures, age models and mechanisms of global change. In: Williams, M., Haywood, A.M., Gregory, F.J., Schmidt, D.N. (Eds.), Deep-Time Perspectives on Climate Change: Marrying the Signal from Computer Models and Biological Roxies. Geological Society of London, London, UK, pp. 323–349.
Strong, N., Paola, C., 2006. Fluvial landscapes and stratigraphy in a flume. The Sedimentary Record 4, 4–8.
Teixell, A., Muñoz, J.A., 2000. Evolución tectono-sedimentaria del Pirineo meridional durante el Terciario: una síntesis basada en la transversal del río Noguera Ribagorçana. Revista de la Sociedad Geológica de España 13, 251–264 (in Spanish).
Thomas, E., Zachos, J.C., 2000. Was the late Paleocene thermal maximum a unique event? GFF 122, 169–170.
Tierney, J.E., Poulsen, C.J., Montañez, I.P., Bhattacharya, T., Feng, R., Ford, H.L., Hönisch, B., Inglis, G.N., Petersen, S.V., Sagoo, N., Tabor, C.R., Thirumalai, K., Zhu, J., Burls, N.J., Foster, G.L., Goddéris, Y., Huber, B.T., Ivany, L.C., Turner, S.K., Lunt, D.J., McElwain, J. C., Mills, B.J.W., Otto-Bliesner, B.L., Ridgwell, A., Zhang, Y.G., 2020. Past climates inform our future. Science 370, 6517. https://doi.org/10.1126/science.aay3701.
Van de Lageweg, W.I., Van Dijk, W.M., Kleinhans, M.G., 2013. Morphological and stratigraphical signature of floods in a braided gravel-bed river revealed from flume experiments. Journal of Sedimentary Research 83, 1033–1046.
Ventra, D., Nichols, G.J., 2013. Autogenic dynamics of alluvial fans in endorheic basins: outcrop examples and stratigraphic significance. Sedimentology 61, 767–791.
Wright, V.P., Marriott, S.B., 1996. A quantitative approach to soil occurrence in alluvial deposits and its application to the Old Red Sandstone of Britain. Journal of the Geological Society 153, 907–913.
Zachos, J.C., Dickens, G.R., Zeebe, R.E., 2008. An early Cenozoic perspective on greenhouse warming and carbon-cycle dynamics. Nature 451, 279–283.
Zellman, K.L., Plink-Björklund, P., Fricke, H.C., 2020. Testing hypotheses on signatures of precipitation variability in the river and floodplain deposits of the Paleogene San Juan Basin, New Mexico, U.S.A. Journal of Sedimentary Research 90, 1770–1801.